RSC Advances

PAPER

View Article Online
View Journal | View Issue

Cite this: *RSC Adv.*, 2026, **16**, 1008

Repurposing waste plastic into a sustainable adsorbent for removing synthetic dye: experimental, optimization and theoretical modeling

Nadeen Eldomiaty,[a] Elsayed Elbayoumy,*[a] Mohamed M. Aboelnga[ab] and Mohamed R. Mostafa*[a]

Plastic waste, particularly polyethylene terephthalate (PET), poses a significant environmental threat due to its persistence and non-biodegradability. This study presents a sustainable approach to repurposing recycled PET bottles into activated carbon for the efficient removal of Brilliant Green (BG) dye from aqueous solutions. The synthesized adsorbent was characterized by FTIR, BET, XRD, XPS, and FESEM analyses, confirming a high surface area (403 m^2 g^{-1}) and abundant functional groups that are favorable for adsorption. Under optimized conditions of 5 mg L^{-1} initial dye concentration, pH 7, 0.1 g adsorbent dose, 298 K, and 120 min contact time, the material achieved a removal efficiency of 99.3%. Adsorption followed pseudo-second-order kinetics and was fitted both Langmuir and Freundlich isotherm models, indicating combined physical and chemical interactions. Thermodynamic parameters revealed a spontaneous and endothermic process, while regeneration tests demonstrated excellent stability over five cycles. Density functional theory (DFT) analysis indicated that preferential adsorption occur through π–π stacking and donor–acceptor interactions. Box–Behnken design (BBD) optimization further validated the model's predictive accuracy. Overall, this work provides both dual environmental benefits by transforming PET waste into a cost-effective, and eco-friendly adsorbent for sustainable dye removal and water purification.

Received 8th November 2025
Accepted 18th December 2025

DOI: 10.1039/d5ra08601a

rsc.li/rsc-advances

1 Introduction

One of the most urgent environmental issues of the twenty-first century is the buildup of plastic waste. Globally every year, millions of tons of plastic are manufactured, and a significant portion ends up in landfills or aquatic ecosystems, where their persistence and resistance to natural degradation lead to long-term ecological damage.[1,2] Plastic debris not only disrupts terrestrial and marine life but also contributes to micro plastic contamination endangers human health and food chains.[3] Among these plastics, PET is a significant contributor because of its widespread useful for packaging, particularly beverage bottles, and its slow degradation rate.[4] Addressing this plastic accumulation problem requires innovative recycling and upcycling approaches that transform waste into value-added products, while simultaneously mitigating environmental hazards.

In parallel, with the rapid industrial expansion witnessed in recent decades, water pollution caused by harmful organic dyes has appeared as a serious environmental and health issue that requires in-depth study.[5,6] Industrial dyes, heavily used across various sectors such as textiles, plastics, printing, and paper manufacturing, are often discharged in large quantities into water bodies without adequate treatment.[7] This leads to significant deterioration in water quality and poses a direct threat to both human health and aquatic life.[8] These dyes are difficult to remove using traditional procedures because of their considerable resistance to biodegradation and chemical stability.[9] Additionally, they increase toxicity levels and chemical oxygen demand (COD), thereby disrupting vital environmental processes such as photosynthesis in aquatic ecosystems.[10] A clear example for the hazards posed by such compounds is the Brilliant Green (BG) dye which, widely used in industrial for dyeing silk, wool, cotton and synthetic fibers, providing bright and stable coloration and in biomedical contexts, it has been used as a topical antiseptic for minor wounds, abrasions and skin infections.[11,12] BG dye is known for causing severe health effects, including permanent eye damage, as well as its toxic impact on aquatic organisms.[13–16] Accordingly, there is a pressing need to investigate this form of pollution and to explore effective methods for treating industrial wastewater containing such dyes in order to safeguard both environmental and human health.[17]

[a]*Chemistry Department, Faculty of Science, Damietta University, Damietta, 34517, Egypt. E-mail: ramzy1950@du.edu.eg; sayedelbayoumy@du.edu.eg; nadeeneldomiaty@du.edu.eg*

[b]*King Salman International University, Faculty of Basic Sciences, Ras Sudr, 46612, South Sinai, Egypt. E-mail: mohamed-aboelnga@du.edu.eg*

To achieve this aim, various treatment technologies have been developed which including biological methods utilizing microorganisms, flocculation and coagulation, chemical and electrochemical oxidation, as well as membrane filtration and adsorption techniques. These approaches rely on a combination of physical, chemical, and biological mechanisms aimed at effectively reducing or removing dye concentrations, thereby minimizing toxic effects and improving the quality of treated water for safe disposal or potential reuse.[18–22]

Adsorption is considered to be among the most popular and successful methods for treating waste water, because of its low cost, high efficiency, operational simplicity, and environmental safety.[23,24] Its advantages are particularly significant while comparing with the restrictions of other methods of treatment, as clogging of membranes and expensive of membrane cleaning, difficulties in catalyst recovery in photo catalysis, and the complexity of advanced oxidation processes.[25,26] Adsorption offers a fast, sludge-free approach capable of removal of different contaminants, including arsenic, synthetic dyes, and heavy metals, while allowing for the recovery and reuse of both pollutants and adsorbents.[27–31] The characteristics of the utilized adsorbent material have a significant impact on this method' efficacy.[32] For this purpose, a wide diversity of adsorbents have been investigated, including carbon-based substances like activated carbon, natural materials such as clay minerals and zeolites, bio-based materials derived from plant residues and agricultural waste, and synthetic options like polymers and nanocomposites.[33–37]

Natural substances have increasingly gained recognition as cost-effective, environmentally friendly and effective dye removal adsorbents from wastewater.[38–40] Among these, materials made of clay as montmorillonite, bentonite, and kaolinite are known for their large surface areas and ion-exchange potential.[41] Natural zeolites have also been widely adopted due to their porous frameworks and cation exchange capabilities.[42] In addition, agricultural residues including rice husks, wood sawdust, banana peels, and coconut shells have shown notable adsorption performance due to their surface-active functional groups.[43–46] Biopolymers like chitosan and alginate further contribute significantly to dye removal, owing to their reactive sites that bind pollutants effectively.[47,48] The broad availability and functional versatility of these natural materials position them as promising solutions for sustainable wastewater treatment technologies.

Because of their low production costs and adaptability, plastics including polypropylene (PP), polyvinyl chloride (PVC), and polyethylene (PE) are indispensable in modern life.[49,50] However, plastics cause significant environmental issues due to their persistence and accumulation, particularly in oceans.[51–53]

Nowadays, PET is recognized as the thermoplastic polymer with the most usage due to its excellent physio-chemical properties, including high tensile strength, low thermal expansion and chemical resistance.[54] The increased demand of PET in many fields such as bottle beverages, food packaging, medical devices electrical and textile industries lead to rapid accumulation of these wastes thus creating serious environmental pollution problems.[55] Due to the growing demand for plastic bottles, PET consumption has increased at a rapid rate over time.

It is noteworthy that PET bottles are among the well-collected plastic waste materials, making them perfect for industrial use. Polymer wastes including plastic are mainly being recycled *via* three different routes: mechanical, energy and chemical technologies.[56,57] In the mechanical method, the waste material is transformed into a new polymer product while its molecular structure remains unchanged.[58] Energy recycling involves the use of incineration technology to produce thermal energy.[59] Chemical recycling involves the conversion of plastic waste into relatively new compounds when they are used as industrial feedstocks.[60]

Due to high carbon content within the skeletons of plastic wastes, several authors in the literature have reported PET waste as a good option for recycling into useful carbon based compounds such as graphene.[61,62] Porous carbons are used for capture of CF_4 (ref. 63) and carbon microspheres are employed for adsorption.[64] In the past five years, activated carbon produced from using post-consumer plastic wastes have evolved and become a target to achieve a friendly technology to prepare relatively inexpensive carbon material with good adsorption capacity for industrial utilization instead of commercial activated carbons.[65–67]

In this study, synthesized activated carbon was derived from plastic bottle waste by way of a carbonization and chemical activation process and thereafter used as an adsorbent to extract BG dye from watery solutions. A thorough characterization of the material was conducted utilizing FTIR, BET, XRD, XPS, and FESEM analysis. The effect of various operational factors, including adsorbent dose, temperature, initial dye concentration, pH, and contact time was thoroughly examined. In addition to kinetics of adsorption, isotherm models, and parameters of thermodynamics, they were analyzed to better understand the mechanism of adsorption and optimize the process. Using DFT simulations, the interaction mechanism between the investigated dye and the activated carbon adsorbent has been clarified. A regeneration study was performed to assess the material's reusability. Moreover, the Box–Behnken design-based Response Surface Methodology (RSM) was used to model and optimize the adsorption conditions. Overall, this approach helps to reduce pollution of plastic while offering low-cost efficient remedy for environmental cleanup by removing dyes from industrial wastewater.

2 Materials and methods

2.1. Materials

PET waste from plastic bottles was collected from local sources at New Damietta City, Egypt, and employed as a raw material for adsorbent preparation. Sodium hydroxide (NaOH), sodium chloride (NaCl) and potassium nitrate (KNO_3) with 98% purity were acquired from Almasria for chemicals (Egypt). Brilliant green dye which has a molecular formula $C_{27}H_{34}N_2O_4S$, was purchased from Aldrich Chemicals. Every chemical was used just as it was delivered, requiring no additional purification.

2.2. Activated carbon synthesis using wasted plastics

PET plastic from waste bottles was gathered and carefully cleaned with distilled water to get rid of any labels or contaminants. After

being left for drying overnight, small portions were cut out of the bottles, then placed in a crucible and heated to 400 °C for three hours in a muffle furnace. After cooling to room temperature, the resulting charred material was ground into a fine powder to obtain the carbonized material.

Activated carbon (AC) was prepared by chemically activating the carbonized material with sodium hydroxide (NaOH) at various C : NaOH weight ratios, including 1 : 0.5, 1 : 1, 1 : 2, and 1 : 3, respectively. Every mixture was agitated and left to soak at room temperature for 24 hours. After that, the samples were filtered, thoroughly washed with distilled water, and dried. The remaining solid materials underwent three hours of thermal treatment at various temperatures: 300, 400, 500, and 600 °C. The samples were dried and kept for later use in adsorption tests after being further cleaned with distilled water until a neutral pH of was reached.

2.3. Theoretical investigation

To further elucidate the adsorption mechanism, computational simulations were conducted to explore the interaction between surface of activated carbon and dye molecules. A representative structural fragment of the activated carbon was constructed and its interaction with the dye was investigated through density functional theory (DFT) calculations using Gaussian09.[68] Geometry of *t* dye–activated carbon complex was fully optimized by applying the B3LYP[69–73] functional together with the 6-31G basis set, a strategy that has proven reliable in our earlier computational studies on different chemical systems[74,75] and has also been widely validated in previous DFT investigations on graphene-based and doped-graphene systems.[76–80] Moreover, this combination of methodology has been successfully employed for the treatment of similar chemical systems and types of analysis. The activated carbon was modeled as a finite polycyclic aromatic hydrocarbon cluster composed of 66 atoms. The basal plane consists of fused hexagonal carbon rings, with all edge carbon atoms saturated by hydrogen to prevent artificial boundary effects. To simulate the chemical heterogeneity typically found in experimentally activated carbon, the model incorporates two ether (C–O–C) oxygen atoms embedded within the basal plane and three carbonyl (C═O) groups positioned along the surface. These oxygenated functionalities provide chemically relevant adsorption sites and capture the reactivity trends of partially oxidized graphene. The entire model was treated as neutral, with a total charge of zero, and all structures were fully optimized before adsorption calculations. This functionalized graphene framework thus offers a realistic and chemically diverse platform for accurately evaluating drug–surface interaction energetics. The binding energy (E_{bind}) is defined as the following:

$$E_{bind} = E_{AC/BG} - (E_{AC} + E_{BG})$$

Here, E_{AC} represents the energy of the activated carbon, E_{BG} molecules is the energy of the drug molecule, and $E_{AC–BG}$ molecules is the energy of the activated carbon after interacting with the drug molecule to form the corresponding complexe. Moreover, (HOMO and LUMO), the frontier molecular orbitals were generated with Gauss View to provide deeper insight into the possible electronic interactions governing the adsorption behavior. The graphene oxide adsorbent was modeled in its neutral state, incorporating ether oxygen functionalities along with carbonyl groups, in accordance with the experimental characterization data.

3 Data presentation and discussion

3.1. Optimization AC preparation variables

Within the scope of the present work, an attempt has been made to optimize the process parameters that lead to the production of activated carbon with better adsorption removal. The influences of NaOH : C impregnation ratio as well as the activation temperature on the percentage dye removal BG are shown in SI Fig. (S1 and S2). Fig. (S1) shows the effects of the NaOH : C impregnation ratio as the % removal of BG with other factors such as activation temperature and time of activation are fixed at 500 °C and 3 h, respectively. The results showed a clear enhancement in dye removal efficiency with increasing NaOH : C ratio. Specifically, the removal percentage increased from 38.29% at the 1 : 0.5 ratio to 85.86% at the 1 : 3 ratio. As illustrated in SI Fig. S1, dye removal efficiency shows a slight increase at lower NaOH : C ratios (from 0.5 to 2), followed by a more pronounced increase at higher ratio, indicating that higher alkali loading enhance adsorption performance. This improvement could be attributed to the establishment of a structure that is more porous, which leads to increased surface area at higher NaOH concentrations, along with the formation of more alkoxide functional groups on the carbon surface. These functional groups provide negatively charged active sites that enhance the electrostatic interaction with the cationic BG dye molecules[81,82]

To further optimize the adsorbent, the effect of activation temperature was investigated by subjecting the activated carbon to thermal treatment at different temperatures ranging from 300 °C to 600 °C, keeping the impregnation ratio and activation time fixed at 1 : 3 and 4 h, respectively. As indicated in Fig. S2, a strong positive correlation was observed between the activation temperature and percentage dye removal. The percentage BG removal increased from 53.70% at activation temperature 300 °C to 96.60% removal for the sample activated at 600 °C. At higher activation temperatures, moisture, light organic compounds, and unstable oxygen-containing groups were released from the carbon matrix, which led to the formation of internal pores and a significant increase in the specific surface area, providing more active sites for dye adsorption.[83] In addition, high-temperature treatment promotes the formation or exposure of functional groups such as –OH and –CHO on the carbon surface. These groups enhance adsorption efficiency through electrostatic interactions and hydrogen bonding with the cationic dye molecules.[84]

3.2. Adsorbent characterization techniques

3.2.1. Characterization using FTIR. Spectrum of the activated carbon derived from PET by FTIR exhibited several

characteristic absorption bands that indicate the existence of many reactive groups retained after activation process as shown in Fig. 1a and Table 1. Notably, absorption bands at 1725 cm^{-1}, which are assigned to vibrational stretching of the carbonyl bond (C═O), indicating the presence of ester, indicating that some of the original ester linkages from PET may have been retained during activation.[74] 1589 cm^{-1} is the absorption peak that corresponds to aromatic C═C stretching vibrations. Suggesting partial preservation of aromatic structure from the original PET.[75,76] Additional peaks were observed at 1383 cm^{-1}, 1271 cm^{-1}, and 1120 cm^{-1}. The band at 1383 cm^{-1} is attributed to the symmetric bending of CH_3 groups, while the peak at 1271 cm^{-1} corresponds to C–O stretching vibrations of ester linkages. The absorption at 1120 cm^{-1} may also be assigned to C–O stretching, indicating the presence of oxygen-containing functional groups.[77] In the fingerprint region, prominent bands were detected at 831, 720, and 615 cm^{-1}. The absorption at 831 cm^{-1} is related to out-of-plane bending vibrations of aromatic C–H bonds, characteristic of *para*-substituted benzene rings. The peak at 720 cm^{-1} is attributed to the rocking vibrations of $-(CH_2)_n-$ groups, suggesting remnants of aliphatic chains. The complex structure of the carbon matrix generated during activation is further supported by the band at 615 cm^{-1}, which corresponds to C–C skeletal vibrations or aromatic ring deformations.[78,79]

3.2.2. Characterization by XPS. To examine the surface chemistry, including elemental distribution and functional moieties, XPS analysis was carried out on the activated carbon produced from PET waste. The survey spectrum (Fig. 1b) revealed distinct peaks attributed to carbon (C 1s) and oxygen (O 1s), appearing at characteristic binding energies near 285.31 eV and 533.12 eV, respectively. Quantitative analysis showed that the surface was predominantly composed of carbon (86%) and oxygen (14%). These elements are indicative of the surface chemical structure of the activated material. Further insight into the nature of the surface functionalities was obtained through high-resolution spectra as shown in Table 2. The spectrum corresponding to the C1s level (Fig. 1c) shows the presence of three major peaks positioned at approximately 288.69 eV, 286.18 eV, and 284.73 eV are observed peaks attributable to C═O/O–C═O, C–O, and C–C/C═C, respectively. The observed peaks confirm the existence of various oxygen-containing species on the surface of the activated carbon derived from PET.[80] The prominent signal at 284.73 eV reflects a high content of sp^2-hybridized carbon, which is indicative of

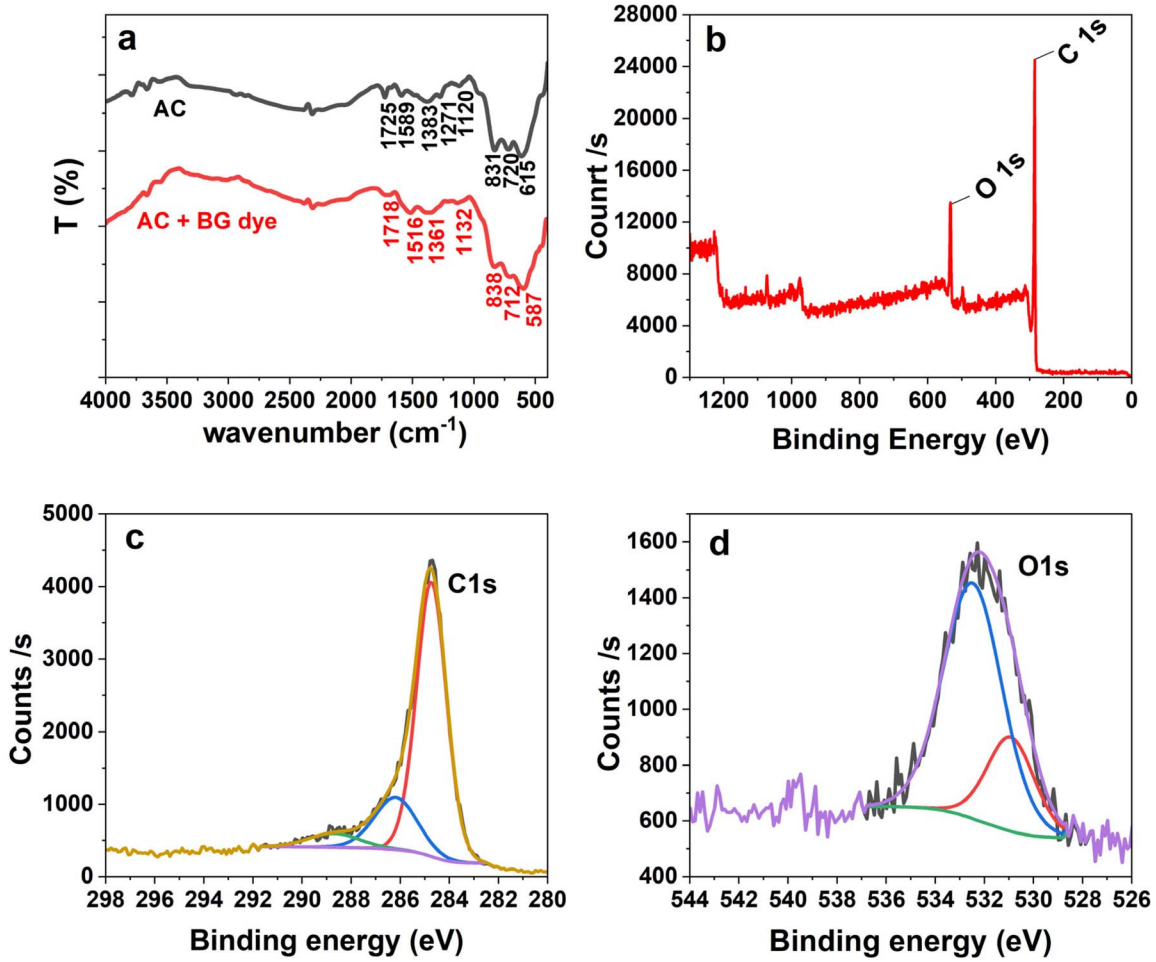

Fig. 1 FTIR spectra of activated carbon before and after adsorption (a); XPS analysis of activated carbon: presence of C and O in structure by survey scan (b), C 1s spectrum (c), and O 1s spectrum (d).

Table 1 Results of FTIR analysis

Wavenumber (cm^{-1})	Assignment	Functional group/Interpretation
1725	C═O stretching	Indicates presence of ester groups; partial retention of PET ester linkages.[85]
1589	Aromatic C═C stretching	Suggests partial preservation of aromatic structure from PET.[77,78]
1383, 1271 and 1120	CH_3 symmetric bending, C–O stretching (esters) and C–O stretching	Evidence of methyl containing groups, ester linkages and oxygen-containing groups and presence of oxygenated functional groups respectively.[79]
831, 720 and 615	Fingerprint region with aromatic C–H out-of-plane bending, $(CH_2)_n$– groups and C–C skeletal vibrations/aromatic ring deformation	Characteristic of *para* substituted benzene rings, remnants of aliphatic chain segments and complex carbon matrix formed during activation respectively.[86,87]

Table 2 Results of XPS analysis

Binding energy (eV)	Spectral region	Functional group
284.73	C 1s	C–C/C═C
286.18	C 1s	C–O
288.69	C 1s	C═O/O–C═O
531.09	O 1s	C═O
532.47	O 1s	C–O

a graphitic structure and suggests the partial formation of graphene-like domains within the material. The O 1s spectrum (Fig. 1d) reveals two distinct peaks at binding energies of 531.09 eV and 532.47 eV. The first peak corresponds to oxygen doubly bonded to carbon (C═O), indicating the presence of carbonyl or carboxyl groups. The second peak is attributed to single-bonded oxygen species (C–O), such as hydroxyl or ether functionalities.[81,82]

3.2.3. XRD analysis. By employing X-ray diffraction (XRD), the crystalline structure of synthesized activated carbon made from PET was examined. A resulting pattern of diffraction, as illustrated in Fig. 2a, reveals two prominent peaks at 2θ values of 23.3° and 43.7°. The peak centered at approximately 23.3° corresponds to the (002) diffraction plane, indicative of graphene-like layered structures with limited crystallinity. Meanwhile, the peak observed at 43.7° is credited to the[100] planes, feature of the pointing out a short-range order of stacked graphene sheets.[94] The broadness and relative intensity of these peaks suggest an overall amorphous structure with embedded graphene domains. These findings confirm the coexistence of amorphous carbon and graphene features within the synthesized material, which suggests that the activation process successfully generated a disordered structure favorable for adsorption application.[88–93]

3.2.4. Textural properties of tested sample. By BET analysis that depends on nitrogen adsorption/desorption measurements, the pore and surface area characteristics of synthesized carbon that is activated were investigated. As depicted in Fig. 2b, the resulting isotherm of activated carbon is consistent with a Type IV profile that is usually connected to materials that are mesoporous. The material appeared to have a specific surface area with 403.00 $m^2\ g^{-1}$, indicating an extensive porous network that enhances its adsorption capacity and such mesoporous characteristics and high surface area are crucial for improving mass transfer and providing sufficient accessibility to adsorption site. The volume of liquid N_2 deposited close to saturation is used to compute the total pore volume. (V_p, mL g^{-1}) that has been found to be 0.299 mL g^{-1}. The mean pore radius ($\bar{r}_p$) was measured from the relationship:[3]

$$\bar{r}_p(\text{Å}) = \frac{2V_p \times 10^4}{S_{BET}} \quad (1)$$

The value of $\bar{r}_p$ was found to be 9.5 Å. More information was estimated by using the α_s method adopted by Sing *et al.*, that employing the data of adsorption on a well-defined carbon with nonporous.[95] From a plot of volume of N_2 adsorbed (V_a) *versus* α_s values (at the same p/p^0), one can derive the total surface area (S_t^α) from the slope of the first straight segment intersecting the origin and estimate the non-micropore surface area (S_n^α) from the slope of the later linear segment, *i.e.*, a mesoporous surface area, while micropore surface area was calculated from:

$$S_{micro}^\alpha = S_t^\alpha - S_n^\alpha.$$

The micropore volume (V_{micro}^α) was estimated from the latter line's intersection with the V_a axis. Assuming negligible volume due to macropore, the mesopore volume was found from: $V_{meso}^\alpha = V_p - V_{mico}^\alpha$. In a Table 3, the textural parameters obtained from α_s method are also included in. The results that presented in a Table 1 show the coexistence of micropore as well as mesopore structure for the activated carbon under investigation. The S_t^α value correlates well with the S_{BET} value confirming a correct choice of the standard isotherm used in the analysis. The closeness between the two values can be taken as evidence for the correctness of a calculated sample's surface area. So, prepared activated carbon can be classified as mesoporous in nature.[96] In addition, presence of a distinct hysteresis loop further confirms the presence of mesopores within structure, which are commonly observed in materials suitable for dye adsorption and environmental remediation applications.

3.2.5. FESEM analysis. Activated carbon made from PET was tested for surface morphology using Field Emission

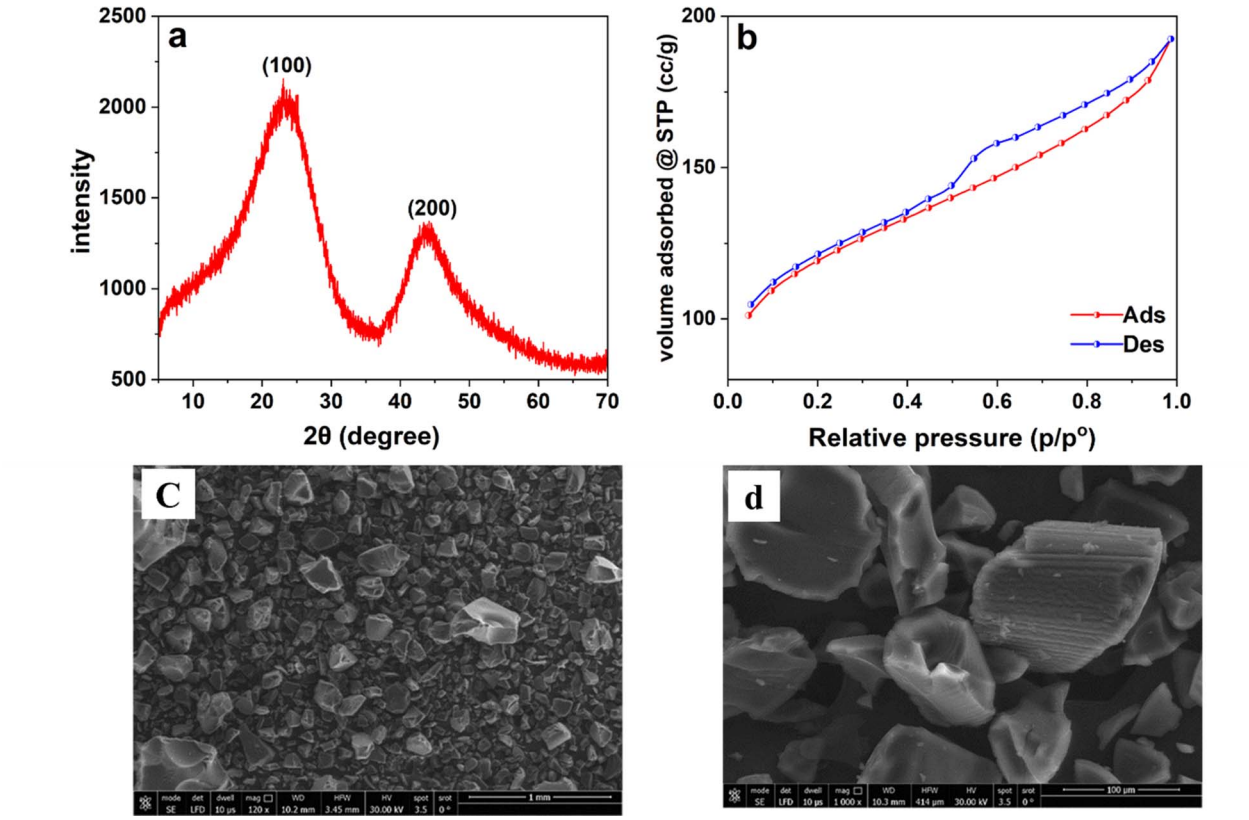

Fig. 2 XRD pattern of activated carbon (a); activated carbon isotherm by N_2 adsorption–desorption (b) and FESEM images of activated carbon with different scales: 1 mm (c) and 100 μm (d).

Scanning Electron Microscopy (FESEM), as well as corresponding micrographs are illustrated in Fig. 2c and d. The FESEM images at various magnifications reveal a rough, heterogeneous, and irregular surface structure composed of aggregated particles. This disordered morphology indicates the existence of a highly established network of porous, and this helps to provide more surface area and makes active adsorption sites more accessible. Such structural characteristics are particularly advantageous for removing of dye from water as example of adsorption processes.

3.3. Adsorption batch experiment

3.3.1. Adsorbent dosage effect. By changing the amount of adsorbent from 0.02 to 0.1 g in dye solution with an initial concentration of 7.5 ppm, under neutral pH and ambient temperature for 2 hours, the impact of the activated carbon dose on the removal efficiency of BG dye was investigated. As demonstrated in Fig. 3a, increasing an adsorbent dose caused the dye removal efficiency to significantly increase between 46.60% into 99.80%. This enhancement can be described by a rise in an available surface area and a greater number of sites that are active for adsorption provided by a higher amount of carbon. But the adsorption capacity (q_e) per mass unit of adsorbent reduced from 1.89 to 0.81 mg g^{-1} with increasing adsorbent dose, likely because of the reduced percentage of accessible surface to dye molecules, which restricts the amount of adsorbent that can be absorbed per gram.[97,98] The optimum adsorbent dosage was found to be 0.1 g, which maximized dye removal, which is crucial for practical wastewater treatment applications.

3.3.2. Impact of concentration of dye. The effect of BG dye initial concentrations on its adsorption behavior using activated carbon is shown in Fig. 3b. Since dye concentration increased from 3 to 30 ppm, a noticeable decline in the removal efficiency was found, decreasing starting with 92.60% for 63.30%. This reduction can be understood by the carbon surface's restricted quantity of active adsorption sites; at higher concentrations of dye, an increased amount of dye molecules

Table 3 Textural parameters of activated carbon derived from PET bottles

S_{PET} m^2 g^{-1}	S_t^{α} m^2 g^{-1}	S_n^{α} m^2 g^{-1}	S_{micro}^{α} m^2 g^{-1}	V_n^{α} cm^3 g^{-1}	V_{micro}^{α} Cm^3/g	V_p cm^3 g^{-1}	$\bar{r}_p$ Å	V_n^{α}/V_p	V_{micro}^{α}/V_p
403	410	181.8	228.2	0.153	0.146	0.299	9.5	0.51	0.49

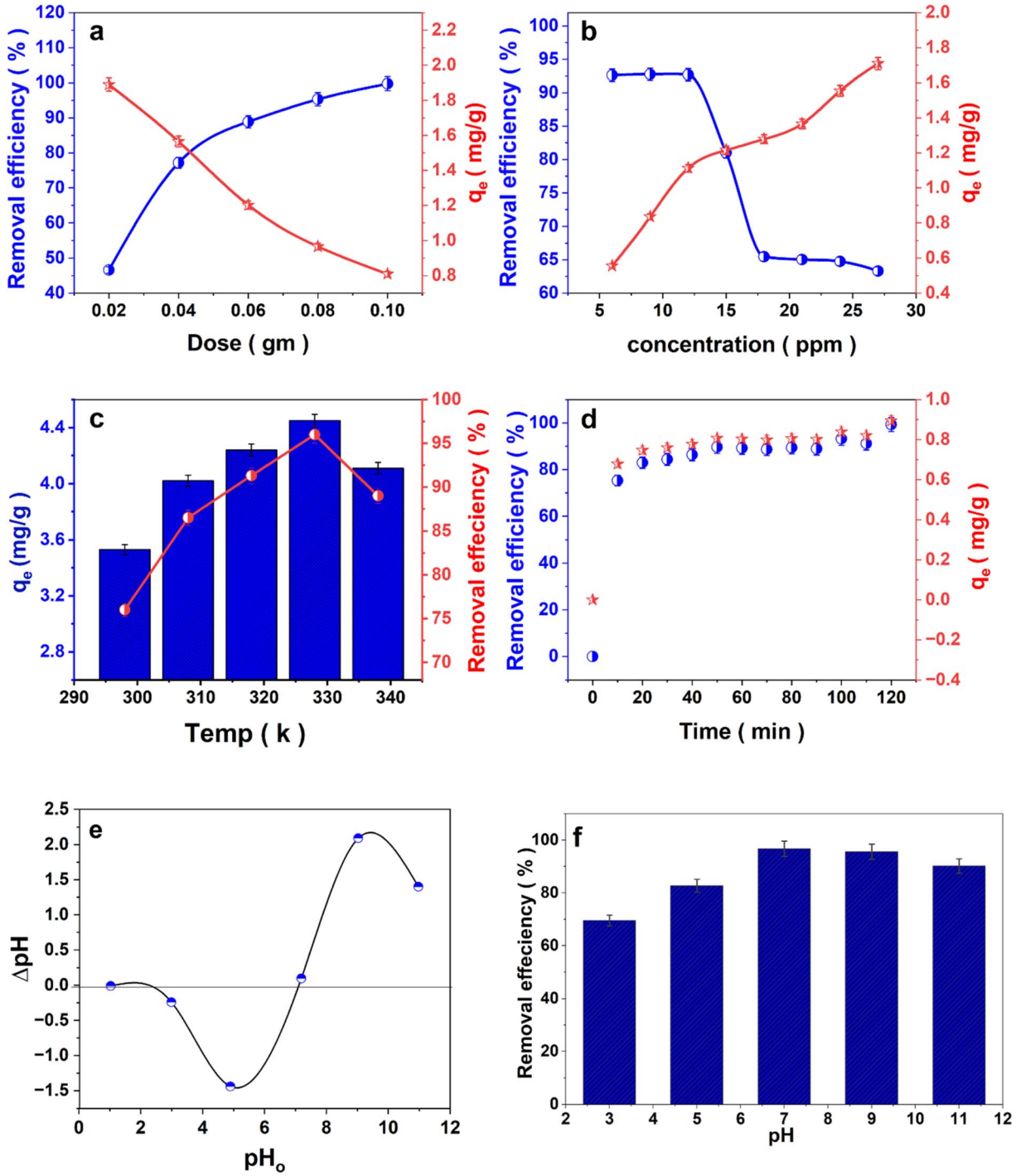

Fig. 3 Impact of dosage of activated carbon on BG dye adsorption (a); impact of the initial BG concentration on the process of adsorption (b); impact of temperature on BG adsorption onto activated carbon (c); contact time's impact on BG's adsorption onto activated carbon (d); pH_{Pzc} of activated carbon (e) and how pH affects BG's ability to adhere to activated carbon (f). Adsorption conditions: pH (from 3 to 11), initial concentration (from 3 to 30 mg L^{-1}), time (from 0 to 120 min), temperature (from 298 to 328 k) and dose (from 0.02 to 0.1 gm).

increases the rivalry locations. The extra dye in the solution is not absorbed once the sites are saturated.[99] However, the value of q_e expanded by 0.55 into 1.70 mg g^{-1} with higher initial concentrations. This increase reflects the greater opportunity for each gram of adsorbent to interact with more molecules of dye present in solution, leading to an increased loading until the adsorbent gets close to its maximum capacity for adsorption.[100] The optimum initial dye concentration was determined to be 5 g L^{-1}, providing a favorable balance between mass transfer driving force and available active sites. This behavior highlights the importance of initial dye concentration in determining adsorbent loading and site saturation.

3.3.3. Impact of contact time. Over a period of 5 to 120 minutes, the impact of contact time on the BG dye's adsorption was examined, while other experimental factors were maintained constant, including temperature, pH, shaking speed, initial concentration of dye, and adsorbent dosage. As shown in Fig. 3d, both dye removal efficiency (%R) and capacity of adsorption (q_e) exhibited a continuous increase with rising time. The first 20 minutes saw a rapid adsorption, after which there was a discernible drop in the adsorption rate until the system achieved. This trend can be accounted for by the large number of accessible active sites on the activated carbon surface at the beginning of the process, which facilitates fast dye uptake. As time progresses, these active sites become gradually occupied by dye molecules, resulting in a slower adsorption rate until no significant changes occur, indicating the attainment of equilibrium.[101] An optimal contact time of 120 minutes was sufficient to achieve maximum adsorption. The observed trend reflects the typical kinetics of heterogeneous carbon surfaces and emphasizes the material's efficiency in rapid dye uptake.

3.3.4. Impact of temperature. The experiments were carried out in temperature range of 298 to 338 K, although other factors including pH, shaking rate, initial BG dye concentration, contact period, and adsorbent dosage remained constant. As shown in Fig. 3c, the rise in temperature from 298 to 328 K led to a noticeable improvement in both the %R and q_e of the BG dye. Specifically, %R increased from 76% to 96%, while q_e rose from 3.53 mg g^{-1} to 4.45 mg g^{-1}. However, when the temperature was raised above 328 K, both the %R and the q_e began to decrease, about values dropping to 89% and 4.11 mg g^{-1}, respectively. Because the dye molecules have more kinetic energy at higher temperatures, which speeds up their movement, this initial increase in adsorption performance can be explained. Thereby enhancing collisions with surface of activated carbon and improving rate of adsorption. Additionally, higher temperatures may help overcome energy barriers, enhancing the interaction between the activated carbon's adsorption sites and the BG dye molecules. Furthermore, elevated temperatures promote the dye molecules' migration

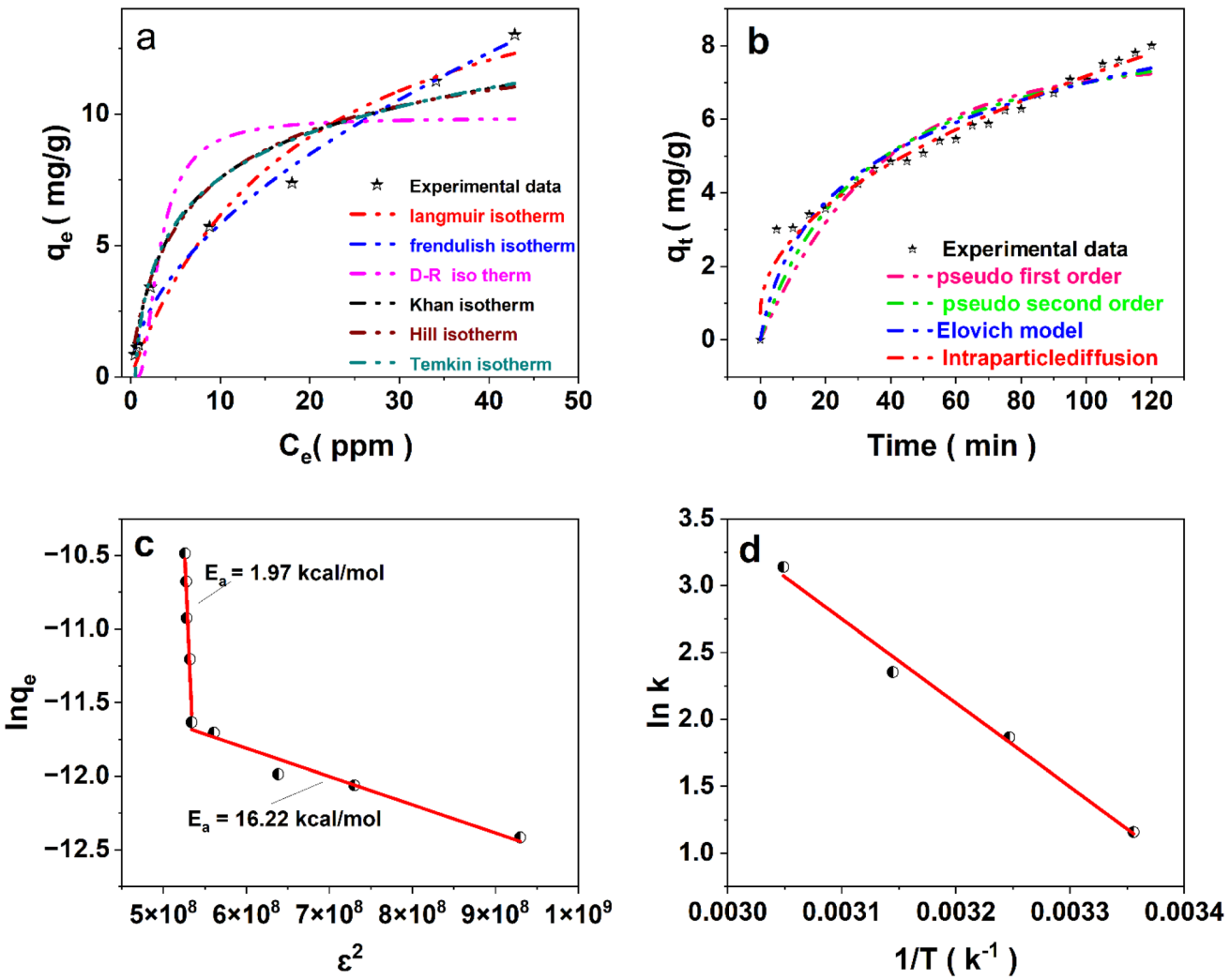

Fig. 4 Adsorption isotherms of BG activated carbon (a), Models of BG's adsorption kinetics onto activated carbon (b), Dubinin–Radushkevich model (c) as well as the BG dye adsorption onto activated carbon plot of ln K against 1/T (d).

from the bulk solution to the surface of adsorbent, contributing to more effective dye removal.[102] Nonetheless, with temperature continues to rise, the sites of adsorption on the activated carbon approach saturation, causing reduction in removal efficiency and potentially triggering and desorption of dye molecules, disrupting an equilibrium in favor of desorption.[103]

3.3.5. (pH_{Pzc}) point of zero charge and pH effect. (pHpzc), which denotes the pH at which all active sites are electrically balanced and the adsorbent's surface charge becomes neutral, was measured experimentally using the described method[76] To evaluate this parameter, a series of 10 mL solutions of KNO_3 (0.1 M) were prepared at initial values of pH adjusted within the variety of 2 to 12 by using NaOH (0.1 M) and HCl (0.1 M). Subsequently, each solution received 0.02 g of activated carbon, and the mixtures were stirred for a full day at room temperature. Following equilibration, the final pH values were noted, and the initial pH was plotted against the difference between the initial and final pH values (ΔpH). The pH_{pzc} is the value at which ΔpH = 0. As presented in Fig. 4, the pH_{pzc} of the synthesized activated carbon was discovered to be 7. This result indicates that at pH less than 7, the activated carbon surface was charged by positive. While at pH more than 7, the surface became charged by negative.

The impact of pH on BG dye's adsorption onto activated carbon was illustrated in Fig. 3e. As we can note, the removal efficiency exhibited an increase between pH 3 and 7, where pH 7 was shown to have the maximum dye removal. Beyond pH 7, the removal efficiency slightly decreased. The cationic nature of BG dye, which maintains its positive charge in aqueous conditions, explains this behavior. In acidic pH, a high concentration of protons (H^+) rivals dye cations for limited sites of adsorption at the surface of the activated carbon, causing lowering of the efficiency of adsorption. The adsorbent surface becomes more negatively charged as the pH rises, which strengthens the electrostatic attraction between activated carbon and the dye cations, thereby enhancing adsorption up to pH 7.[104] At alkaline conditions (pH > 7), removal efficiency declines again, which is related to the reduction in positive charge of BG dye and possible electrostatic repulsion, as well as potential structural changes of the dye molecules under basic conditions. These observations highlight those electrostatic forces are the dominant mechanism governing BG dye uptake by activated carbon.[105,106] Consequently, the ideal pH for further adsorption tests was determined to be 7.

3.3.6. Ionic strength's influence. Ionic strength influence on the adsorption of BG dye on activated carbon was examined by changing the NaCl concentration from 0 to 0.5 mol L^{-1} while keeping the initial dye concentration, adsorbent dosage, pH, and temperature constant. As shown in SI Fig. S3, a rise in removal efficiency of BG dye was observed, rising from 83.00% to 96.00% with increasing NaCl concentration, and the observed rise in removal efficiency of dye with rising up to 0.5 mol L^{-1} concentration of NaCl is explained by the salting out effect, which occurs when dye molecules become less soluble in the aqueous phase. As a result, dye molecules tend to aggregate because of physical phenomena like dipole–dipole attractions and van der Waals forces. Increased removal efficiency results from these aggregated dye molecules being more readily adsorbed onto the activated carbon surface. This phenomenon can also be explained by the dye molecules' increased dimerization when the concentration of salt rises. The salt helps to boost the dye adsorption process on the surface of activated carbon by fortifying the intermolecular interactions between the dye molecules.[107]

3.4. Adsorption isotherm

For understanding the type of interactions that occur between adsorbate and adsorbent depends heavily on adsorption isotherms, and for elucidating the underlying adsorption process mechanisms. To gain insight into whether adsorption occurs as a multilayer or

Table 4 BG's isotherm of adsorption onto activated carbon

Isotherm models	Equation form	Parameters and its values	
Langmuir	$= \frac{K \times q_m \times C_e}{1 + K \times C_e \times q_e}$	q_m mg g^{-1}	17.69
		K L mg^{-1}	0.05
		R^2	0.961
Freundlich	$q_e = K \times F \times C_e^{1/n}$	K_F mg g^{-1}	1.67
		$1/n$	0.54
		R^2	0.99
Dubinin–Radushkevich	$q_e = q_m \exp^{-K\,[RT\ln(1+1/C_e)]2}$	q_m mg g^{-1}	9.86
	$E_a = \frac{1}{\sqrt{2K}}$	K mol^2 J^{-2}	3.79×10^{-9}
		R^2	0.56
Khan	$q_e = \frac{q_m \times K \times C_e}{(1 + K \times C_e)^n}$	q_m mg g^{-1}	7.38
		n	0.83
		K	0.37
		R^2	0.99
Temkin	$q_e = B \ln(K \times C_e)$	K L mg^{-1}	2.10
		B	2.48
		R^2	0.92
Hill	$q_e = q_m \times C_e^n/(K + C_e^n)$	q_m mg g^{-1}	14.22
		n	0.77
		K	5.21
		R^2	0.99

monolayer, models of isotherm are provided, along with the strength of the adsorbate–adsorbent affinity and the theoretical maximum capacity of adsorption. In this study, six different models of isotherm were used to evaluate data of experiments and determine the most appropriate representation of adsorption behavior. Langmuir, Dubinin–Radushkevich (D–R), Freundlich, Temkin, Hill, and Khan isotherms are among the models that are used.[108–111]

As seen in Fig. 4a, the applied adsorption isotherm models' non-linear forms, and Table 4 displays the matching parameters derived *via* curve fitting. Langmuir isotherm decided that the adsorption would occur uniformly on the adsorbent surface, exhibiting a monolayer type of adsorption with a uniform distribution of energy levels.[112] As shown, Fig. 4a displays the Langmuir isotherm, and Table (4) provides its parameters, The following formula can be used to determine the separation factor R_L, which is another way to define the Langmuir isotherm: $R_L = \frac{1}{(1 + KC_0)}$. Value of R_L was found to be 0.386 for the tested carbon indicating that the removal of BG is favorable process ($0 < R_L < 1$) with a correlation coefficients (R^2) value of 0.961 which reveal that the Langmuir model effectively describes the adsorption process.

Freundlich isotherm model is a practical model and can be applied in heterogeneous surface system where K_F and n in isotherm equation that presented in Table 4. Corresponding to the adsorbent's adsorption capacity and intensity, respectively. The adsorption process is found to be favorable if n lies in the range of 1–10.[113] The values of adsorption intensity correlation coefficient (R^2) for BG on sample were found to be 1.58 and 0.99 showing that the BG adsorption on PET AC adsorbent matched the Freundlich isotherm closely.

Based on Polanyi's potential theory, Dubinin–Radushkevich (D–R) isotherm is commonly used to characterize adsorption processes on microporous materials. This model assumes that the adsorption energy follows a Gaussian distribution within the pores of the adsorbent. One of its key advantages is the ability to determine the mean free energy of adsorption (E) in order to distinguish between chemical and physical adsorption. Generally, E values less than 8 kJ mol^{-1} are linked to physisorption, while values above this threshold indicate chemisorption.[114]

In the present study, the D–R isotherm was utilized in the BG dye adsorption experiment on activated carbon. Experimental data showed that the adsorption process proceeds through two distinct stages as shown in Fig. 4c. Initially, a low activation energy equal to 1.97 kcal mol^{-1} was observed, indicating that the adsorption at this stage occurs primarily *via* physisorption. This weak interaction is attributed to forces of van der Waals between the surface of the adsorbent and the adsorbate. Subsequently, a marked increase in activation energy to 16.22 kcal mol^{-1} was recorded, suggesting a transition to chemisorption, wherein the surface and the adsorbed molecules develop stronger chemical connections.[115] Such behavior can be explained by taking into account that the molecules of the adsorbate initially adhere to the surface through feeble physical interactions, which thereafter permit them to diffuse or align into advantageous orientations. These initial interactions serve as a preparatory step that facilitates the subsequent formation of covalent or coordinative bonds during chemisorption. Such a sequential adsorption mechanism where physisorption precedes chemisorption is commonly observed in surface reaction processes, particularly when the activation energy is initially insufficient to drive chemical bonding directly.[116]

Others models, including Temkin, Hill, and Khan, were also tested and there results are summarized briefly in Table 4.

3.5. Kinetics of adsorption

It is crucial to comprehend adsorption kinetics for elucidating an underlying adsorption mechanism. This study used a variety of kinetic models, such as (PFORE) the pseudo-first-order, pseudo-second-order (PSORE), intra-particle diffusion (IPD), and Elovich models, to investigate the mechanism and rate-limiting steps of the adsorption process.[117,118]

According to (PFORE) model, the number of accessible active sites on the adsorbent surface determines the adsorption rate; (PSORE) model believes that the predominant mechanism is chemisorption, which involves the adsorbent and the adsorbate exchanging or transferring electrons.[118] Relationship between adsorption capacity and time for each model is depicted in Fig. 4b. Furthermore, the calculated parameters of kinetic with their corresponding R^2 values are summarized in a Table 5.

Also, Table 5 presents an analysis of the R^2 for the PFORE ($R^2 = 0.88$) and PSORE ($R^2 = 0.91$) models shows that the experimental results fits the PSORE model better indicating that this model offers a more realistic depiction of the system under study's adsorption behavior.

The differential chemisorption of BG onto activated carbon was evaluated using the Elovich model. The high correlation coefficient ($R^2 = 0.95$) presented in Fig. 5b and Table 4 confirms the suitability of this model for describing the process. These findings suggest that BG adsorption onto activated carbon follows chemisorption kinetics, with the Elovich equation providing an accurate representation of the adsorption behavior. Mechanism of adsorption of BG dye onto the synthesized carbon that be activated and the possible rate-limiting steps were investigated using the model of (IPD) and results exhibits highly accord with it ($R^2 = 0.98$). The adsorption process may go through several stages, such as bulk diffusion, film diffusion, and intra-particle diffusion, either separately or in combination,

Table 5 BG adsorption kinetics onto activated carbon

Kinetics model	Equation form	Parameters	
PFORE	$q_t = q_e(1 - e^{K t})$	q_e mg g^{-1}	7.51
		K min^{-1}	0.03
		R^2	0.88
PSORE	$q_t = \frac{q_e^2 \times K_2 \times t}{1 + q_e \times K_2 \times t}$	q_e mg g^{-1}	9.31
		K_2 g (mg^{-1}.min)	0.003
		R^2	0.91
Elovich	$q_t = \frac{1}{\ln(\alpha \times \beta \times t + 1)}$	β g mg^{-1}	0.44
		α mg g^{-1} min	0.49
		R^2	0.95
IPD	$q_t = K_{diff} t^{0.5} + C$	K_{diff} mg g^{-1} min$^{-0.5}$	0.64
		C	0.72
		R^2	0.98

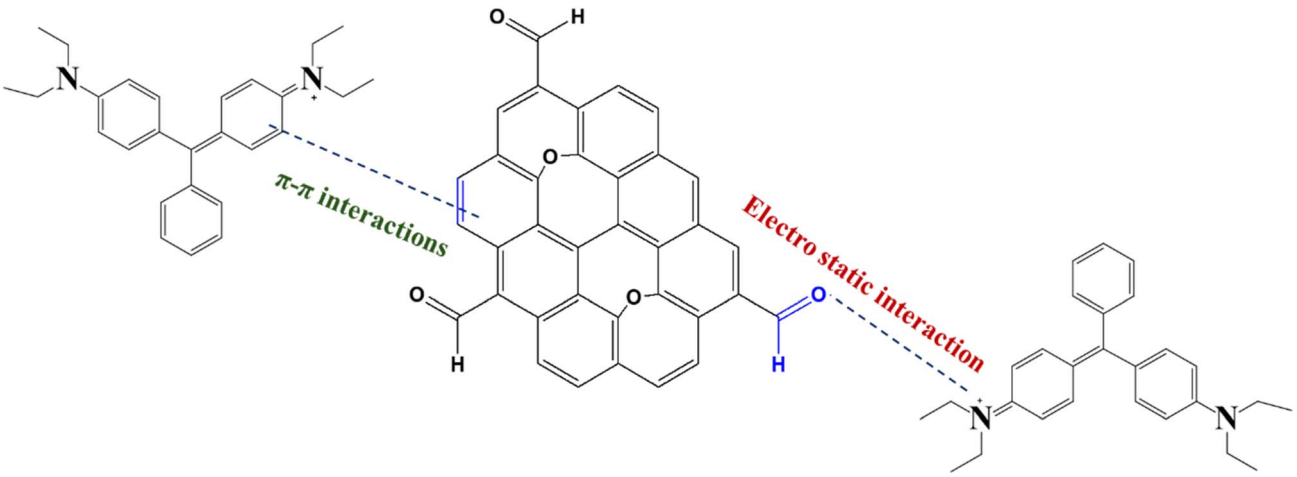

Fig. 5 Mechanism interaction between activated carbon from PET and BG dye.

depending on the model's underlying assumptions. This observation indicating that IPD is essential to the transport mechanism that allows BG dye to be adsorbed onto activated carbon.

3.6. Adsorption thermodynamics

In order to examine the thermodynamic behavior of BG dye adsorption onto activated carbon, important thermodynamic parameters such as the enthalpy change ($\Delta H°$), entropy change ($\Delta S°$), and Gibbs free energy change ($\Delta G°$) were calculated. These parameters were calculated based on experimental adsorption data collected over a temperature range of 298 K to 328 K. Values were derived by the equation of van't Hoff, that allows for an evaluation of spontaneity, heat exchange, and randomness changes associated with process of adsorption.

$$K = \frac{C_{AC}}{C_e} \tag{2}$$

$$\ln K = -\frac{\Delta H}{R} \times \frac{1}{T} + \frac{\Delta S}{R} \tag{3}$$

$$\Delta G = -T\Delta S + \Delta H \tag{4}$$

In which, R denotes an ideal gas constant, which has a value of 8.314 J mol^{-1} K^{-1}, T indicates the temperature on the Kelvin scale, K expresses the thermodynamic constant related to equilibrium, the term C_e describes the concentration of Brilliant Green (BG) dye that remains in the solution once equilibrium is reached, measured in mg L^{-1} and, C_{AC} reflects the equilibrium adsorption capacity, representing the amount of dye taken up per liter of solution, also in mg L^{-1}.

The thermodynamic parameters were assessed using the relationship between the inverse of temperature ($1/T$) and the natural logarithm of the equilibrium constant ($\ln K$), as shown in Fig. 4d. The enthalpy change ($\Delta H°$) and entropy change ($\Delta S°$) were calculated from the slope and intercept of the resulting linear plot, respectively. A suitable thermodynamic equation was then used to determine the Gibbs free energy change ($\Delta G°$) at various temperatures. Table 6 provides a summary of the computed values for each thermodynamic parameter.

While the negative values of $\Delta G°$ at all temperatures under study suggest that the adsorption is spontaneous, the positive value of $\Delta H°$ verifies that the BG dye's adsorption onto the activated carbon is an endothermic process. Furthermore, the observed drop in $\Delta G°$ as the temperature rises points to improved adsorption feasibility at higher temperatures. The displacement of water molecules and structural reorganization at the adsorbent surface may be the cause of the positive value of $\Delta S°$, which indicates an increase in randomness at the solid–liquid interface during the adsorption process.

Table 6 Thermodynamic variables of BG activated carbon adsorption

	Variables		
T (K)	$\Delta G°$ kJ mol^{-1}	$\Delta H°$ kJ mol^{-1}	$\Delta S°$J mol^{-1} K^{-1}
298	−54.98	52.19	184.66
308	−56.82		
318	−58.67		
328	−60.52		

3.7. Mechanism of adsorption process

3.7.1. Experimental investigation. After process of adsorption of BG dye, we perform analysis by FTIR to illustrate possible way that the dye and adsorbent molecules interact. As presented in Fig. 1a, a noticeable shifts and intensity changes in key functional group regions was observed, indicating active participation in the adsorption process of surface groups. A distinct peak that was ascribed to the stretching vibration C=O of ester groups and seen at 1725 cm^{-1} before adsorption, shifted to 1718 cm^{-1} after dye adsorption, suggesting the dye molecules' electrostatic interaction to the carbonyl surface groups. The stretching vibration C=C aromatic initially located in 1589 cm^{-1} changed to 1516 cm^{-1}, further supporting π–π interactions between Brilliant Green's aromatic rings and surface of carbon. Moreover, CH_3 symmetric bending peak changed from 1383 cm^{-1} to 1361 cm^{-1}, also the stretching spectra of C–O slightly changed from

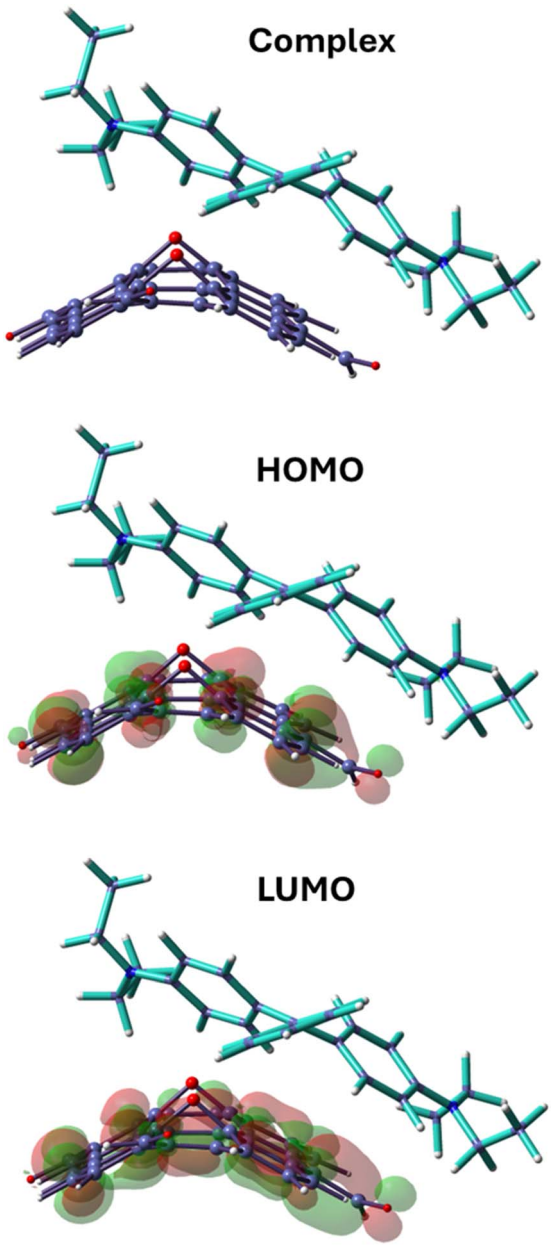

Fig. 6 Molecular geometry optimization and frontier molecular orbital distribution (HOMO and LUMO) of the brilliant green (BG) dye adsorbed on activated carbon (AC).

1120 cm^{-1} to 1132 cm^{-1}, both indicating potential chemical or physical interaction containing functional groups that are oxygenated on the adsorbent surface. These spectral changes strongly suggest that π–π interactions and electrostatic bonds played significant roles in Brilliant Green's adsorption mechanism on PET-derived carbon that activated *n* as illustrated in the proposed mechanism in Fig. 5.

3.7.2. Theoretical investigation. The DFT-optimized model of the activated carbon (AC)–brilliant green (BG) dye complex confirms that the dye preferentially assumes parallel configuration with respect to surface of AC, promoting strong noncovalent π–π interactions occur between the aromatic components of the dye and the delocalized π-electron framework of AC (Fig. 6). This geometry allows for enhanced orbital overlap and stabilizes the adsorption complex.

Frontier molecular orbital analysis further clarifies the interaction mechanism. The HOMO is predominantly localized on the AC surface, particularly around the aromatic carbon regions and oxygen functionalities, whereas the LUMO is also distributed mainly across the AC framework, with minimal contribution from the BG dye. This orbital arrangement indicates that the electronic activity during excitation or charge transfer is largely governed by the AC surface itself. The BG dye, while structurally stabilized through π–π stacking, does not directly contribute to the LUMO, suggesting that its role is more as a stabilizing adsorbate rather than as an active electron acceptor in this configuration. In fact, the calculated binding energy for this interaction is found to be −34.14 kcal mol^{-1} indicating a favorable interaction which supports our investigated mechanism.

These finding highlights that a dominant adsorption mechanism of BG dye on AC is π–π stacking reinforced by noncovalent interactions, rather than strong donor–acceptor chemisorption. The localization of both HOMO and LUMO on AC underscores the intrinsic electronic activity of the AC surface, which plays the primary role in governing adsorption and possible subsequent electronic processes.

3.8. Regeneration study

To evaluate the prepared activated carbon's stability and reusability for adsorption of BG from water, a series of Cycles of adsorption and desorption were performed, and the corresponding results are shown in Fig. 7a. The data show a gradual decrease in removal efficiency over five consecutive cycles, with the percentage of dye removal declining from approximately 99% in the first cycle to 90% by the fifth. FTIR spectroscopy was employed to analyze the activated carbon before and after the recycling process, as shown in Fig. 7b. The FTIR spectra revealed no noticeable alterations to the distinctive peaks, suggesting that functional groups of an adsorbent remained stable during reuse. These findings confirm the strong reusability, chemical stability, and reliable performance of activated carbon in BG dye removal under the applied experimental conditions. Although a slight reduction was observed, the material maintained a relatively high level of performance throughout the cycles. These findings confirm the adsorbent's reasonable stability and reusability under the tested conditions, supporting the possibility of using it practically in repeated adsorption operations.

3.9. Optimization process by statistical analysis

3.9.1. Design of Box Behnken. (BBD) Box Behnken Design was employed to investigate the exchanges between multiple experimental variables and for adsorption process optimization. This model approach was selected because of its efficiency in minimizing the number of experimental runs required while still enabling accurate modeling and prediction of the system's response.[119] In this study, BBD was applied to evaluate the combined impacts of initial dye concentration, adsorbent dose, and contact time on the effectiveness of BG dye removal using

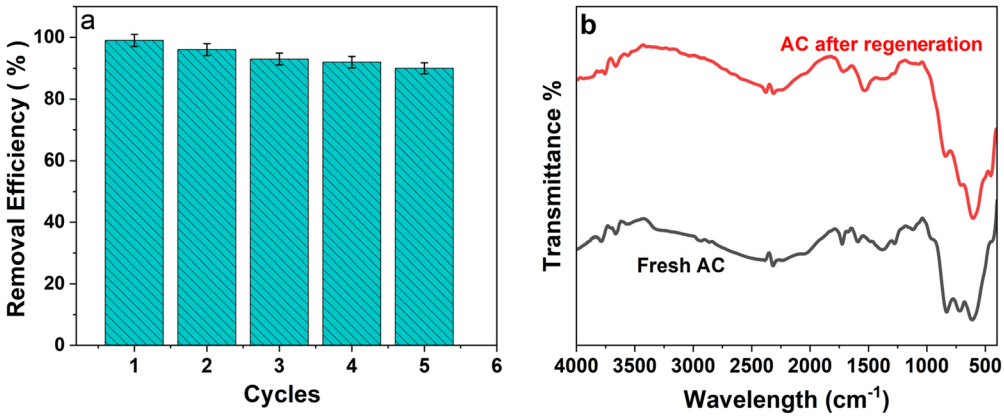

Fig. 7 Regeneration efficiency of activated carbon for the BG's adsorption (a) and the activated carbon's infrared spectra prior to and following the regeneration experiment (b).

activated carbon. The design enabled systematic analysis of factor interactions with reduced experimental effort and cost, while maintaining high prediction accuracy.

The total number of experimental runs produced was 17 using the BBD to assess the impact of selected variables on process of adsorption. The adsorption capacity (q_e) had been chosen for the response variable for evaluating the system's performance. The results of the experimental trials, along matching values that predicted, are summarized in Table 7. Relationship between the response and the input factors was modeled by a second-order polynomial equation, as presented in eqn (5).

$$q_e = 5.74 + 3.19 \times A - 14.77 \times B + 4.98 \times C - 4.69 \times AB - 0.3610 \times AC - 4.96 \times BC - 0.9150 \times A^2 + 11.89 \times B^2 + 2.68 \times C^2 \quad (5)$$

Where the parameters A, B, and C represent contact time (min), adsorbent dose (mg), and dye concentration (mg L^{-1}), respectively.

The predictive model expressed in terms of coded variables, as presented in eqn (5), enables estimation of the response at specific levels of each independent variable. In the coded form, low, center and high stages of the factors are automatically portrayed as −1, 0 and +1, respectively. This format allows for easy comparison of the relative influence of each factor based on the magnitude and sign of their coefficients. Furthermore, eqn (6) presents the model in actual (uncoded) units, where t is time, D is doe, and C is dye concentration. These actual units allow for direct interpretation of the practical effects of factor levels on the adsorption capacity.

$$q_e = 17.76871 + 0.293785 \times t - 0.678587 \times D + 0.172711 \times C - 0.002604 \times t \times D - 0.000451 \times t \times C - 0.005516 \times D \times C - 0.000572 \times t^2 + 0.005873 \times D^2 + 0.006703 \times C^2 \quad (6)$$

The real equation, stated by way of the original units of each variable, can be used to predict the response for specific values

Table 7 Experimental and expected results of the activated carbon's adsorption capacity

	Factors			q_e (mg g^{-1})		
Run	Time (min)	Dose (mg)	Concentration mg L^{-1}	Experimental data	Predicted value	Residual value
1	10	55	50	9.38	9.656	−0.27
2	50	55	30	5.74	5.74	0.00
3	10	100	30	2.64	3.44	−0.80
4	50	55	30	5.74	5.74	0.00
5	50	100	50	6.64	5.56	1.08
6	90	100	30	2.40	0.46	1.94
7	50	55	30	5.74	5.74	0.00
8	10	10	30	21.67	23.61	−1.94
9	90	55	50	12.30	15.32	−3.02
10	90	10	30	40.18	39.38	0.80
11	50	55	30	5.74	5.74	0.00
12	50	10	10	24.07	25.15	−1.08
13	50	10	50	47.25	45.03	2.22
14	90	55	10	6.36	6.09	0.27
15	50	100	10	3.316	5.53	−2.22
16	50	55	30	5.745	5.74	0.00
17	10	55	10	2	−1.02	3.02

Table 8 Response surface ANOVA results

Source	Sum of square	Df	Mean square	*F*-value	*P*-value	Remark	Standard error
Intercept							1.06
Model	2854.25	9	317.14	56.33	< 0.0001	Significant	
A-Time	81.57	1	81.57	14.49	0.0067		0.84
B-Dose	1745.70	1	1745.70	310.07	< 0.0001		0.84
C-Concentration	198.26	1	198.26	35.22	0.0006		0.84
AB	87.89	1	87.89	15.61	0.0055		1.19
AC	0.52	1	0.52	0.09	0.7698		1.19
BC	98.59	1	98.59	17.51	0.0041		1.19
A^2	3.53	1	3.53	0.63	0.4548		1.16
B^2	595.50	1	595.50	105.77	< 0.0001		1.16
C^2	30.26	1	30.26	5.38	0.0535		1.16
Residual	39.41	7	5.63				
Lack of fit	39.41	3	13.14				
Pure error	0.0000	4	0.0000				
Cor total	2893.66	16					

of the experimental factors. In this form, the inputs must be provided in their actual measured units. However, this version of the model is not suitable for comparing the relative influence of the individual factors, as the intercept does not match the center point of the design space, and coefficients are scaled based on the units of measurement.

(ANOVA) analysis was conducted for examination a statistical relevance of parameters affecting the process of adsorption of BG on AC and to uncover key interactions among variables within the experimental framework.[120] This approach also aided in confirming the reliability of the developed predictive equation. Moreover, the method was instrumental in visualizing the relationships between process inputs and system behavior using graphical outputs. The outcomes of this statistical evaluation are detailed in Table 8. The importance of individual terms was assessed through their *p*-values matching, where values less than 0.05 reflect the meaningful contribution to improving the accuracy and explanatory strength of the fitted regression equation.

As illustrated in Table 6, the high *F*-value ($F = 56.33$) alongside a *p*-value less than 0.05 confirms the statistical relevance of the developed model.[121] The coefficient of determination (R^2) reflects how well the variability in the model of regression captures the response variable. In this study, value of R^2 was 0.9864, while the adjusted R^2 was 0.97, both indicating strong agreement between the experimental results and the predicted values. The closeness between the predicted R^2 (0.78) and the adjusted R^2 (0.97), with a difference less than 0.2, supports the reliability of the model's predictive power. Moreover, the Adequate Precision (Adeq-Prec) value, this stands for the ratio of signal to noise, was found to be 25.31 well above the desirable threshold of 4 demonstrating that the model provides a sufficient signal and can be effectively used to explore space of design. Additionally, the average variation of actual data points from expected values is represented by the standard deviation of 2.37, further confirms the consistency and accuracy of the model, reinforcing its suitability for predictive and optimization purposes (Table 9).

3.9.2. Response surface plots. Three-dimensional response plots of surface and their corresponding two-dimensional contour diagrams were utilized for envision and interpret the combined impacts of important process factors on BG dye's adsorption capacity. These graphical representations were generated using Design-Expert software to examine how variations in adsorbent initial concentration, dosage, and contact time influence adsorption behavior onto activated carbon.[122]

As illustrated in Fig. 8, the interactions among these parameters significantly affect the system's performance. In Fig. 8A, the adsorption capacity improved with increasing contact time; however, excessive adsorbent dosage resulted in a decline in capacity, likely due to overlapping of active sites. Fig. 8B shows that both higher initial concentration of dye and longer contact time enhanced the capacity of adsorption. Lastly, as depicted in Fig. 8C, while an increase in initial dye concentration led to improved dye uptake, raising the adsorbent dose beyond a certain level caused a reduction in adsorption efficiency. These findings reflect the importance of optimizing parameter combinations to achieve maximum adsorption performance.

3.9.3. Analyzing the Box Behnken model's suitability. As shown in Fig. 9a, the close alignment of the data, the model's ability to precisely estimate the adsorption capacity is confirmed by the points surrounding the diagonal line, which show a strong agreement between the experimental and

Table 9 Overview of the statistical data for various BG adsorption models onto activated carbon

Source	Std. Dev	Sequential *p*-value	Press	R^2 value	R^2 adjusted	R^2 predicted	Remark
Linear	8.17	0.0010	1618.01	0.7000	0.6308	0.4408	
2FI	8.25	0.4681	2671.41	0.7646	0.6234	0.0768	
Quadratic	**2.37**	**0.0001**	**630.57**	**0.9864**	**0.9689**	**0.7821**	**Suggested**
Cubic	0.0000	<0.0001		1.0000	1.0000		**Aliased**

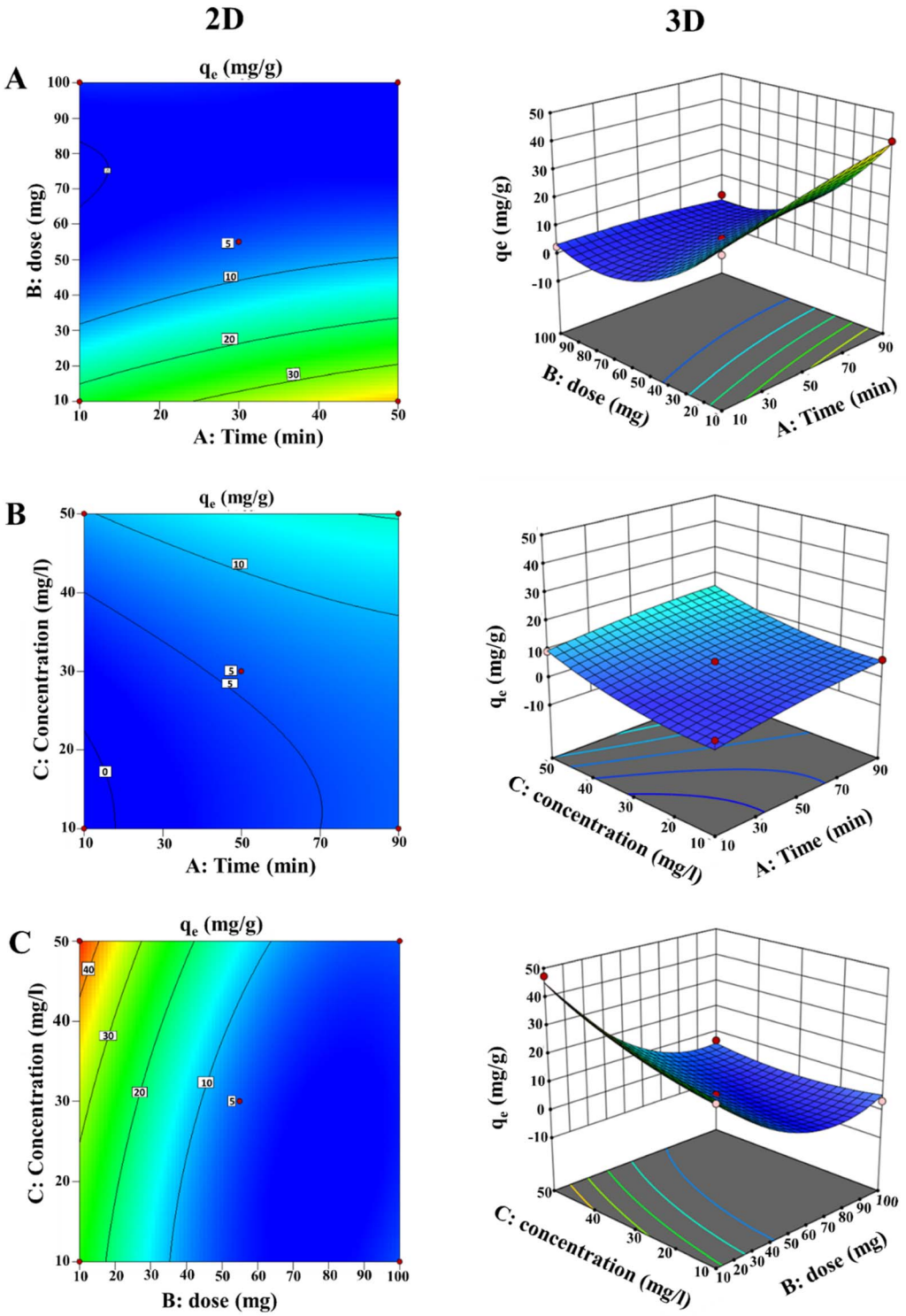

Fig. 8 The relationship between dose and time is depicted by contour plots and a three-dimensional response surface (A), time and initial concentration (B) and dose and initial concentration (C) for the use of activated carbon to remove BG dye.

anticipated values. Fig. 9b illustrates the connection between the expected values and the externally studentized residuals. When assessing the regression model, these standardized residuals which are computed by dividing the difference between observed and anticipated responses by the standard error are a crucial diagnostic tool.

Further assessment is illustrated in Fig. 9c and d, where the externally studentized residuals are plotted against the experimental run numbers. This visualization helps detect any irregular patterns or fluctuations in residual values across the sequence of experiments. Identifying such trends is useful for uncovering potential sources of systematic error whether in the

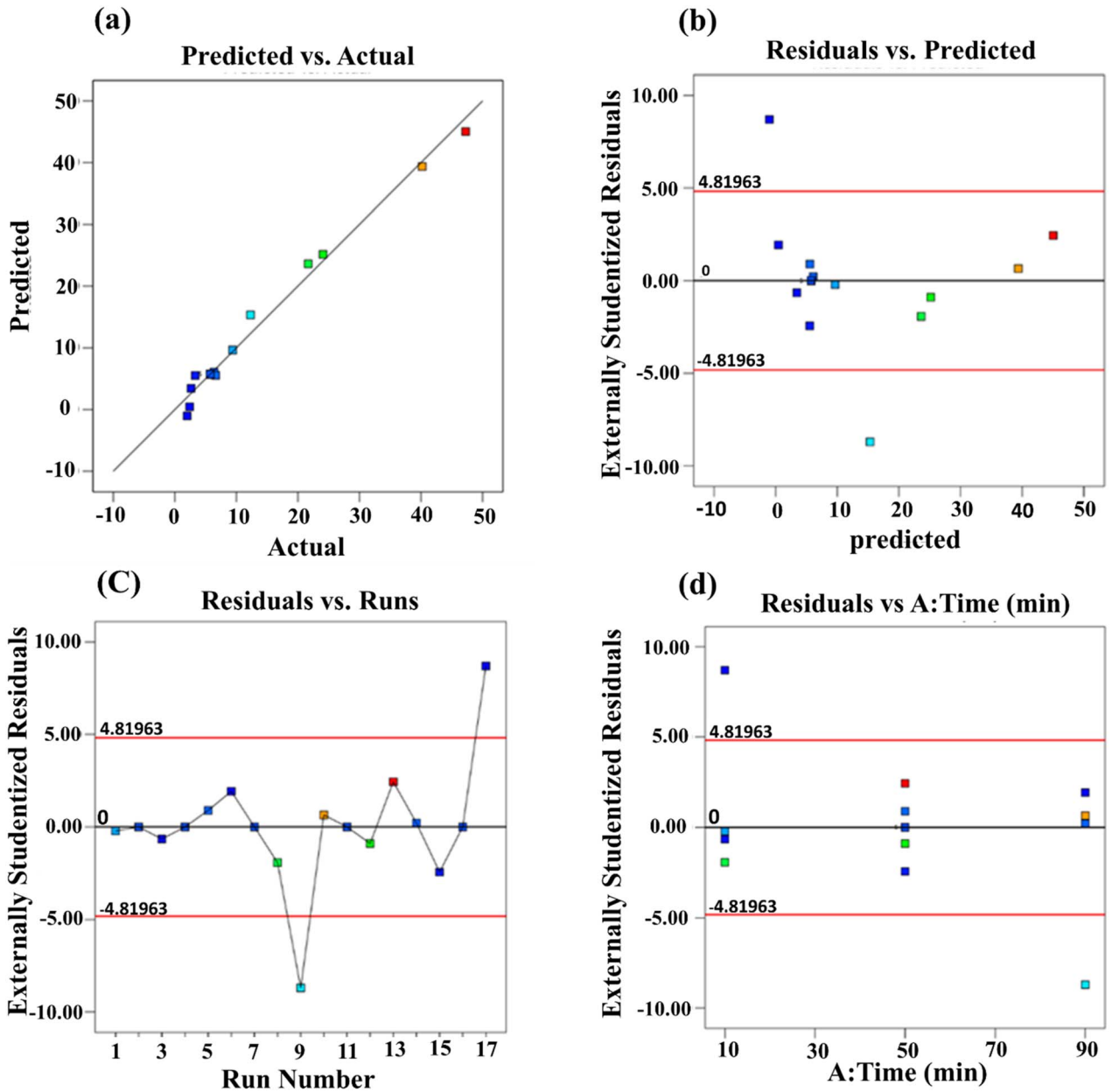

Fig. 9 Comparing the experimental and projected adsorption capacities (a–d).

experimental procedure, data recording, or measurements taken between runs. Recognizing and addressing these patterns is essential for maintaining the validity and consistency of the experimental findings.

3.9.4. Optimization conditions by BBD. The adsorption process was optimized using Response Surface Methodology (RSM) based on the Box–Behnken Design (BBD). Numerical optimization was performed with the primary objective of maximizing the adsorption capacity (q_e) while remaining within the boundaries of the experimental design domain. Using the validated quadratic model, the optimization routine identified the precise combination of variables that yielded the highest predicted adsorption performance. The model-derived optimum conditions were determined as follows: contact time (A) = 74.74 min, adsorbent dose (B) = 10.40 mg, and initial dye concentration (C) = 48.53 mg L^{-1}. Under these optimized parameters, the maximum predicted adsorption capacity was 47.83 mg g^{-1}.

It is important to note that the optimization performed in the experimental investigation targeted removal efficiency rather than adsorption capacity. Experimentally, the material achieved a 99.3% removal efficiency under the conditions of 5 mg L^{-1} initial dye concentration, pH 7, 0.1 g adsorbent dose, 298 K, and 120 min contact time. The difference between the optimal conditions obtained experimentally and those predicted by the BBD model reflects the difference in optimization objectives: maximizing removal percentage in the laboratory *versus* maximizing q_e in the numerical RSM model.

These findings confirm that while experimental optimization maximizes removal efficiency under practical operating conditions, the BBD-based RSM model identifies the conditions that

Table 10 Comparison between the activity of AC with another reported adsorbent

No.	Adsorbent	Reaction condition			Removal (%)	Ref.
		BG conc. (mg L^{-1})	Dose (gm)	Time (min)		
1	Activated carbon from PET	12	0.1	120	99.3	This study
2	PET/sodium alginate composite	20	0.05	120	95.6	123
3	Modified clay	20	0.1	60	94.2	124
4	Coconut shell activated carbon	20	0.1	90	98.6	125
5	Activated carbon from durian shell	25	0.1	60	96.6	126
6	Cashew nut activated carbon	20	0.1	120	99.2	127
7	poly(divinylbenzene)	7.5	0.05	120	97.4	106
8	Poly(AN-*co*-AMPS)	7.5	0.1	80	99.5	103
9	Activated carbon material from peanut shells	100	2	360	80.0	128
10	Banana peel activated carbon	10	0.125	75	99.0	129

maximize adsorption capacity (q_e). Together, the two approaches complement each other and provide a more robust and comprehensive evaluation of the adsorption performance of the material.

3.10. Comparison with other reported adsorbents

To assess the adsorption execution of the synthesized PET-based activated carbon for BG dye removal, a comparative analysis was conducted with various adsorbents previously reported in the literature, as summarized in Table 10. Although direct comparison can be limited due to variations in experimental factors such as initial concentration of dye, contact time, and dosage of adsorbent, the PET-derived carbon demonstrated a notably high removal efficiency of 99.30% within comparatively mild circumstances (12 mg L^{-1} concentration of dye, 120 min contact period and dosage of adsorbent with 0.1 g). In comparison, PET/sodium alginate composite achieved 95.6% removal at 20 mg L^{-1} concentration and 120 min contact time; modified clay showed 94.2% efficiency at 20 mg L^{-1} and 60 min; red mud–bagasse biochar reached 89.30% at 50 mg L; activated carbon derived from durian shell exhibited 96.6% at 25 mg L^{-1} in 60 min; cashew nut shell activated carbon achieved 99.20% at 20 mg L^{-1} after 120 min: poly(divinylbenzene) have 97.45% removal efficiency at 7.5 mg L^{-1} and 120 min of contact time: activated carbon material from peanut shells with 80% at 100 mg L^{-1} initial concentration and 370 min contact time: banana peel activated carbon shown 99% with 10 mg L^{-1} and 75 min and AN & AMPS monomers appear 99.5% at 7.5 mg L^{-1} and 80 min. Among all, the PET-based adsorbent not only provided the highest removal efficiency but also did so at shorter contact time and lower dye concentration, which underscores its adsorption effectiveness, operational simplicity, and suitability for practical wastewater treatment applications. Compared to other reported adsorbents, the developed material in this study offers several advantages. It is derived from waste plastic, which makes it a sustainable and eco-friendly option. Additionally, it is low-cost, recyclable, and contributes to addressing environmental pollution by reducing plastic waste.

4 Conclusions

At present work, an effective, affordable, and environmentally friendly adsorbent for the elimination of dangerous BG dye from aqueous solutions was synthesized using activated carbon made from PET waste. Overall, an adsorbent not only exhibited excellent removal efficiency for BG dye but also offered additional advantages including recyclability, low cost, eco-friendliness, and stability. Its preparation from plastic waste adds value by contributing to environmental sustainability and waste management. The adsorbent achieved a favorable specific surface area with 403 m^2 g^{-1}, which greatly enhanced its adsorption performance by providing an extensive porous structure with abundant active sites. Under optimized conditions, a 99.3% maximum dye removal efficiency was achieved at an equilibrium time of 120 minutes. The Freundlich isotherm model provided the best description of the adsorption process according to its R^2 value = 0.99, demonstrating heterogeneous surface adsorption and multilayer development the results imply that the adsorption process may involve both physisorption and chemisorption mechanisms. An initial weak physical interaction likely facilitates the subsequent formation of stronger chemical bonds. This dual-stage behavior highlights the complexity of the adsorption mechanism and indicates that physisorption can act as a precursor to chemisorption under certain conditions according to values of activation energy from isotherm model of D–R. Kinetic data fitted the PSORE model, indicating that the predominant process was chemisorption. The adsorption process was found to be spontaneous and endothermic by thermodynamic study, further supporting the feasibility of using this material in real-world applications. DFT analysis confirmed that brilliant green (BG) dye preferentially adsorbs onto graphene oxide in a parallel orientation, driven by strong π–π stacking and complementary electronic interactions between oxygenated functionalities of the surface and the dye. The HOMO–LUMO distributions revealed a clear donor–acceptor mechanism, where the cationic dye acts as the electron acceptor and graphene as the main electron donor, providing a mechanistic basis for the experimentally observed adsorption efficiency.

Excellent reusability was shown by the adsorbent, which maintained high removal efficiency throughout five consecutive regeneration cycles with little degradation in performance. These findings demonstrate the potential of activated carbon produced from PET as a promising and eco-friendly alternative for large-scale wastewater treatment, combining high adsorption efficiency, thermal stability, and cost-effectiveness.

Author's contribution

Nadeen Eldomiaty: investigation, data curation, calculation, visualization, formal analysis, methodology, writing – original draft. Elsayed Elbayoumy: supervision, conceptualization, validation, formal analysis, investigation, resources, data curation, writing – review & editing. Mohamed M. Aboelnga: supervision, conceptualization, calculation, visualization, analysis, writing – review & editing; Mohamed R. Mostafa: supervision, conceptualization, project administration, writing – review & editing.

Conflicts of interest

The authors declare that they have no known competing financial interests or personal relationships that could have appeared to influence the work reported in this paper.

Data availability

The data that support the findings of this study are available from the corresponding author upon reasonable request.

Supplementary information (SI) is available. See DOI: https://doi.org/10.1039/d5ra08601a.

Acknowledgements

This research did not receive any specific grant from funding agencies in the public, commercial, or not-for-profit sectors.

References

1 P. G. C. Nayanathara Thathsarani Pilapitiya and A. S. Ratnayake, The world of plastic waste: A review, *Cleaner Mater.*, 2024, **11**, 100220.
2 MdG. Kibria, N. I. Masuk, R. Safayet, H. Q. Nguyen and M. Mourshed, Plastic Waste: Challenges and Opportunities to Mitigate Pollution and Effective Management, *Int. J. Environ. Res.*, 2023, **17**(1), 20.
3 T. Muringayil Joseph, S. Azat, Z. Ahmadi, O. Moini Jazani, A. Esmaeili, E. Kianfar, *et al.*, Polyethylene terephthalate (PET) recycling: A review, *Case Stud. Chem. Environ. Eng.*, 2024, **9**, 100673.
4 B. S. Andreasi, D. Tonini, H. Saveyn and T. F. Astrup, Environmental and Socioeconomic Impacts of Poly(ethylene terephthalate) (PET) Packaging Management Strategies in the EU, *Environ. Sci. Technol.*, 2022, **56**(1), 501–511.
5 T. K. Sen, Adsorptive removal of dye (methylene blue) organic pollutant from water by pine tree leaf biomass adsorbent, *Processes*, 2023, **11**(7), 1877.
6 S. Gamoudi and E. Srasra, Adsorption of organic dyes by HDPy+-modified clay: effect of molecular structure on the adsorption, *J. Mol. Struct.*, 2019, **1193**, 522–531.
7 B. Abbou, I. Lebkiri, H. Ouaddari, A. El Amri, F. E. Achibat, L. Kadiri, *et al.*, Improved removal of methyl orange dye by adsorption using modified clay: combined experimental study using surface response methodology, *Inorg. Chem. Commun.*, 2023, **155**, 111127.
8 Y. Tong, Y. Zang, S. Su, Y. Zhang, J. Fang, Y. Yang, *et al.*, Methylene blue intercalated vanadium oxide with synergistic energy storage mechanism for highly efficient aqueous zinc ion batteries, *J. Energy Chem.*, 2023, **77**, 269–279.
9 J. Yu, L. Bai, Z. Feng, L. Chen, S. Xu and Y. Wang, Waste treats waste: Facile fabrication of porous adsorbents from recycled PET and sodium alginate for efficient dye removal, *Chemosphere*, 2024, **355**, 141738.
10 K. A. Adegoke and O. S. Bello, Dye sequestration using agricultural wastes as adsorbents, *Water Resour. Ind.*, 2015, **12**, 8–24.
11 S. Singh, H. Gupta, S. Dhiman and N. K. Sahu, Decontamination of cationic dye brilliant green from the aqueous media, *Appl. Water Sci.*, 2022, **12**(4), 61.
12 A. W. Feinberg, The use of brilliant green in the treatment of chronic ulcers of the skin, *N. Engl. J. Med.*, 1948, **239**(17), 613–615.
13 M. M. Asai and K. Tapadia, Biofabricated magnetic CuO@ Fe3O4 nanocomposites: Synthesis, characterization and Brilliant Green dye removal from aqueous media and its kinetics study, *J. Indian Chem. Soc.*, 2025, **102**(5), 101668.
14 J. Khodayari, K. Zare, O. Moradi, M. Kalaee and N. M. Mahmoodi, Synthesis of eco-friendly carboxymethyl cellulose/metal–organic framework biocomposite and its photocatalytic activity, *J. Photochem. Photobiol., A*, 2024, **446**, 115097.
15 A. Mittal, D. Kaur and J. Mittal, Applicability of waste materials—bottom ash and deoiled soya—as adsorbents for the removal and recovery of a hazardous dye, brilliant green, *J. Colloid Interface Sci.*, 2008, **326**(1), 8–17.
16 K. G. Bhattacharyya and A. Sarma, Adsorption characteristics of the dye, Brilliant Green, on Neem leaf powder, *Dyes Pigm.*, 2003, **57**(3), 211–222.
17 H. Gupta, S. Yadav and N. Singh, Development of hybrid zinc tannate material for toxic cationic brilliant green dye removal from wastewater, *J. Hazard. Mater. Adv.*, 2025, **17**, 100569.
18 M. K. A. Khan, A. S. Abdulhameed, H. Alshahrani and S. Algburi, Chitosan/functionalized fruit stones as a highly efficient adsorbent biomaterial for adsorption of brilliant green dye: Comprehensive characterization and statistical optimization, *Int. J. Biol. Macromol.*, 2024, **263**, 130465.
19 S. Ihaddaden, D. Aberkane, A. Boukerroui and D. Robert, Removal of methylene blue (basic dye) by coagulation-flocculation with biomaterials (bentonite and Opuntia ficus indica), *J. Water Process Eng.*, 2022, **49**, 102952.
20 K. S. Hirpara and U. D. Patel, Quantitative structure–activity relationship (QSAR) models for color and COD removal for some dyes subjected to electrochemical oxidation, *Environ. Technol.*, 2023, **44**(16), 2374–2385.
21 T. Benhalima, W. Chicha and H. Ferfera-Harrar, Sponge-like biodegradable polypyrrole-modified biopolymers for selective adsorption of basic red 46 and crystal violet dyes from single and binary component systems, *Int. J. Biol. Macromol.*, 2023, **253**, 127532.

22 M. Pasichnyk, J. Gaálová, P. Minarik, M. Václavíková and I. Melnyk, Development of polyester filters with polymer nanocomposite active layer for effective dye filtration, *Sci. Rep.*, 2022, **12**(1), 973.
23 R. Pelalak, R. Soltani, Z. Heidari, R. E. Malekshah, M. Aallaei, A. Marjani, *et al.*, Molecular dynamics simulation of novel diamino-functionalized hollow mesosilica spheres for adsorption of dyes from synthetic wastewater, *J. Mol. Liq.*, 2021, **322**, 114812.
24 R. Soltani, A. Marjani and S. Shirazian, A hierarchical LDH/MOF nanocomposite: single, simultaneous and consecutive adsorption of a reactive dye and Cr (vi), *Dalton Trans.*, 2020, **49**(16), 5323–5335.
25 A. C. Sadiq, A. Olasupo, W. S. W. Ngah, N. Y. Rahim and F. B. M. Suah, A decade development in the application of chitosan-based materials for dye adsorption: A short review, *Int. J. Biol. Macromol.*, 2021, **191**, 1151–1163.
26 A. Olasupo and F. B. M. Suah, Recent advances in the removal of pharmaceuticals and endocrine-disrupting compounds in the aquatic system: A case of polymer inclusion membranes, *J. Hazard. Mater.*, 2021, **406**, 124317.
27 S. Dutta, B. Gupta, S. K. Srivastava and A. K. Gupta, Recent advances on the removal of dyes from wastewater using various adsorbents: A critical review, *Mater. Adv.*, 2021, **2**(14), 4497–4531.
28 M. R. Awual, Novel conjugated hybrid material for efficient lead (II) capturing from contaminated wastewater, *Mater. Sci. Eng., C*, 2019, **101**, 686–695.
29 M. R. Awual, Mesoporous composite material for efficient lead (II) detection and removal from aqueous media, *J. Environ. Chem. Eng.*, 2019, **7**(3), 103124.
30 M. R. Awual, T. Yaita, T. Kobayashi, H. Shiwaku and S. Suzuki, Improving cesium removal to clean-up the contaminated water using modified conjugate material, *J. Environ. Chem. Eng.*, 2020, **8**(2), 103684.
31 M. K. Yadav, D. Saidulu, A. K. Gupta, P. S. Ghosal and A. Mukherjee, Status and management of arsenic pollution in groundwater: A comprehensive appraisal of recent global scenario, human health impacts, sustainable field-scale treatment technologies, *J. Environ. Chem. Eng.*, 2021, **9**(3), 105203.
32 X. Hu, Y. Zeng, H. Liu, B. Da, H. Li, B. Hong, *et al.*, Designing interfacial edge microenvironments of cobalt phosphide quantum dots/graphitic carbon nitride to modulate electron delocalization for ultrafast photocatalytic hydrogen evolution, *Chem. Eng. J.*, 2025, 168790.
33 G. Crini and E. Lichtfouse, Advantages and disadvantages of techniques used for wastewater treatment, *Environ. Chem. Lett.*, 2019, **17**(1), 145–155.
34 M. A. M. Salleh, D. K. Mahmoud, W. A. W. A. Karim and A. Idris, Cationic and anionic dye adsorption by agricultural solid wastes: a comprehensive review, *Desalination*, 2011, **280**(1–3), 1–13.
35 A. A. Ahmad and B. H. Hameed, Reduction of COD and color of dyeing effluent from a cotton textile mill by adsorption onto bamboo-based activated carbon, *J. Hazard. Mater.*, 2009, **172**(2–3), 1538–1543.
36 K. M. Manjaiah, R. Mukhopadhyay, R. Paul, S. C. Datta, P. Kumararaja and B. Sarkar. Clay minerals and zeolites for environmentally sustainable agriculture, in *Modified Clay and Zeolite Nanocomposite Materials*. Elsevier; 2019. pp. 309–29.
37 J. Rouquerol, P. Llewellyn and K. Sing, Adsorption by clays, pillared clays, zeolites and aluminophosphates, *APPS*, 2014, 467–527.
38 S. Yuan, N. Lin, J. Zou, Z. Liu, Y. Yu, Y. Ma, *et al.*, Manipulation tribological behavior of Ti6Al4V alloy *via* a duplex treatment of double glow plasma surface molybdenizing-laser surface texturing (LST), *J. Mater. Res. Technol.*, 2020, **9**(3), 6360–6375.
39 S. Niketh and G. L. Samuel, Surface texturing for tribology enhancement and its application on drill tool for the sustainable machining of titanium alloy, *J. Cleaner Prod.*, 2017, **167**, 253–270.
40 Z. Zhang, Z. Xu, J. Wang, W. Wu and Z. Chen, Preparation and characterization of Ir coating on WC ceramic by double glow plasma, *J. Mater. Eng. Perform.*, 2012, **21**(10), 2085–2089.
41 H. N. Tran, S. J. You, A. Hosseini-Bandegharaei and H. P. Chao, Mistakes and inconsistencies regarding adsorption of contaminants from aqueous solutions: a critical review, *Water Res.*, 2017, **120**, 88–116.
42 E. Pérez-Botella, S. Valencia and F. Rey, Zeolites in adsorption processes: State of the art and future prospects, *Chem. Rev.*, 2022, **122**(24), 17647–17695.
43 M. A. M. Salleh, D. K. Mahmoud, W. A. W. A. Karim and A. Idris, Cationic and anionic dye adsorption by agricultural solid wastes: a comprehensive review, *Desalination*, 2011, **280**(1–3), 1–13.
44 O. A. Ioannidou, A. A. Zabaniotou, G. G. Stavropoulos, M. A. Islam and T. A. Albanis, Preparation of activated carbons from agricultural residues for pesticide adsorption, *Chemosphere*, 2010, **80**(11), 1328–1336.
45 U. S. Orlando, A. U. Baes, W. Nishijima and M. Okada, Preparation of agricultural residue anion exchangers and its nitrate maximum adsorption capacity, *Chemosphere*, 2002, **48**(10), 1041–1046.
46 S. Biswas and A. Pal, Application of biopolymers as a new age sustainable material for surfactant adsorption: A brief review, *Carbohydr. Polym. Technol. Appl.*, 2021, **2**, 100145.
47 Y. Vijaya, S. R. Popuri, V. M. Boddu and A. Krishnaiah, Modified chitosan and calcium alginate biopolymer sorbents for removal of nickel (II) through adsorption, *Carbohydr. Polym.*, 2008, **72**(2), 261–271.
48 A. N. Doyo, R. Kumar and M. A. Barakat, Recent advances in cellulose, chitosan, and alginate based biopolymeric composites for adsorption of heavy metals from wastewater, *J. Taiwan Inst. Chem. Eng.*, 2023, **151**, 105095.
49 J. Wang, X. Yuan, S. Deng, X. Zeng, Z. Yu, S. Li, *et al.*, Waste polyethylene terephthalate (PET) plastics-derived activated carbon for CO 2 capture: a route to a closed carbon loop, *Green Chem.*, 2020, **22**(20), 6836–6845.
50 A. E. Schwarz, T. N. Ligthart, E. Boukris and T. Van Harmelen, Sources, transport, and accumulation of

different types of plastic litter in aquatic environments: a review study, *Mar. Pollut. Bull.*, 2019, **143**, 92–100.
51 O. I. Nkwachukwu, C. H. Chima, A. O. Ikenna and L. Albert, Focus on potential environmental issues on plastic world towards a sustainable plastic recycling in developing countries, *Int. J. Ind. Chem.*, 2013, **4**(1), 34.
52 E. J. North and R. U. Halden, Plastics and environmental health: the road ahead, *Rev. Environ. Health*, 2013, **28**(1), 1–8.
53 T. D. Moshood, G. Nawanir, F. Mahmud, F. Mohamad, M. H. Ahmad and A. AbdulGhani, Sustainability of biodegradable plastics: New problem or solution to solve the global plastic pollution?, *Curr. Res. Green Sustainable Chem.*, 2022, **5**, 100273.
54 T. M. Joseph, S. Azat, Z. Ahmadi, O. M. Jazani, A. Esmaeili, E. Kianfar, *et al.*, Polyethylene terephthalate (PET) recycling: A review, *Case Stud. Chem. Environ. Eng.*, 2024, **9**, 100673.
55 P. Sarda, J. C. Hanan, J. G. Lawrence and M. Allahkarami, Sustainability performance of polyethylene terephthalate, clarifying challenges and opportunities, *J. Polym. Sci.*, 2022, **60**(1), 7–31.
56 S. Nandi, S. S. Mahish, S. K. Das, M. Datta and D. Nath, A review of various recycling methods of PET waste: an avenue to circularity, *Polym.-Plast. Technol. Mater.*, 2023, **62**(13), 1663–1683.
57 R. L. Smith, S. Takkellapati and R. C. Riegerix, Recycling of plastics in the United States: plastic material flows and polyethylene terephthalate (PET) recycling processes, *ACS Sustain. Chem. Eng.*, 2022, **10**(6), 2084–2096.
58 M. Frounchi. Studies on degradation of PET in mechanical recycling, in *Macromolecular Symposia*. Wiley Online Library; 1999. pp. 465–9.
59 K. Choudhary, K. S. Sangwan and D. Goyal, Environment and economic impacts assessment of PET waste recycling with conventional and renewable sources of energy, *Procedia CIRP*, 2019, **80**, 422–427.
60 A. Bohre, P. R. Jadhao, K. Tripathi, K. K. Pant, B. Likozar and B. Saha, Chemical recycling processes of waste polyethylene terephthalate using solid catalysts, *ChemSusChem*, 2023, **16**(14), e202300142.
61 W. A. Algozeeb, P. E. Savas, D. X. Luong, W. Chen, C. Kittrell, M. Bhat, *et al.*, Flash graphene from plastic waste, *ACS Nano*, 2020, **14**(11), 15595–15604.
62 B. Liu, Y. Wang, H. Wen, Y. Wang, H. Liu, B. Da, *et al.*, Modulating Surface-Active Hydrogen for Facilitating Nitrate-to-Ammonia Electroreduction on Layered Double Hydroxides Nanosheets, *Adv. Funct. Mater.*, 2025, e19238.
63 X. Yuan, M. K. Cho, J. G. Lee, S. W. Choi and K. B. Lee, Upcycling of waste polyethylene terephthalate plastic bottles into porous carbon for CF4 adsorption, *Environ. Pollut.*, 2020, **265**, 114868.
64 L. Meng, X. Xu, B. Bai, M. Ma, S. Li, N. Hu, *et al.*, Surface carboxyl-activated polyester (PET) fibers decorated with glucose carbon microspheres and their enhanced selective adsorption for dyes, *J. Phys. Chem. Solids*, 2018, **123**, 378–388.
65 C. S. de Castro, L. N. Viau, J. T. Andrade, T. A. P. Mendonça and M. Goncalves, Mesoporous activated carbon from polyethyleneterephthalate (PET) waste: pollutant adsorption in aqueous solution, *New J. Chem.*, 2018, **42**(17), 14612–14619.
66 V. Gómez-Serrano, M. Adame-Pereira, M. Alexandre-Franco and C. Fernández-González, Adsorption of bisphenol A by activated carbon developed from PET waste by KOH activation, *Environ. Sci. Pollut. Res.*, 2021, **28**(19), 24342–24354.
67 I. Pet, M. N. Sanad, M. Farouz, M. M. ElFaham, A. El-Hussein, M. S. A. El-Sadek, *et al.*, Recent developments in the implementation of activated carbon as heavy metal removal management, *Water Conserv. Sci. Eng*, 2024, **9**(2), 62.
68 M. J. ea Frisch, G. W. Trucks, H. B. Schlegel, G. E. Scuseria, R. Ma and J. R. Cheeseman, *et al. Gaussian 16*. Gaussian, Inc., Wallingford, CT, 2016.
69 P. J. Stephens, F. J. Devlin, C. F. Chabalowski and M. J. Frisch, Ab initio calculation of vibrational absorption and circular dichroism spectra using density functional force fields, *J. Phys. Chem.*, 1994, **98**(45), 11623–11627.
70 A. D. Becke, Density-functional thermochemistry. III. The role of exact exchange, *J. Chem. Phys.*, 1993, **98**(7), 5648–5652.
71 J. P. Perdew, M. Ernzerhof and K. Burke, Rationale for mixing exact exchange with density functional approximations, *J. Chem. Phys.*, 1996, **105**(22), 9982–9985.
72 A. Zhu, H. Liu, L. Qiao, B. Liu, K. Liu, C. Luan, *et al.*, Tuning Active Hydrogen on Reconstructed RuO2/Co (OH) 2 Catalysts for Selective Ammonia Synthesis, *Adv. Mater.*, 2025, e15346.
73 H. Liu, Y. Wang, P. Tan, E. C. Dos Santos, S. M. Holmes, H. Li, *et al.*, A Doping-Induced SrCo0. 4Fe0. 6O3/CoFe2O4 Nanocomposite for Efficient Oxygen Evolution in Alkaline Media, *Small*, 2024, **20**(21), 2308948.
74 M. M. Aboelnga, J. J. Hayward and J. W. Gauld, Enzymatic post-transfer editing mechanism of E. coli threonyl-tRNA synthetase (ThrRS): A molecular dynamics (MD) and quantum mechanics/molecular mechanics (QM/MM) investigation, *ACS Catal.*, 2017, **7**(8), 5180–5193.
75 M. M. Aboelnga, J. J. Hayward and J. W. Gauld, Unraveling the critical role played by Ado762′ OH in the post-transfer editing by archaeal threonyl-tRNA synthetase, *J. Phys. Chem. B*, 2018, **122**(3), 1092–1101.
76 M. M. Aboelnga, M. M. Seliem, E. El-Bayoumy and M. El-Tahawy, DFT investigation of dye adsorption on pristine and doped graphdiyne: toward efficient removal of disperse yellow 3 from wastewater, *Nanoscale Adv.*, 2025, **7**(22), 7363–7381.
77 S. Gholami, A. S. Rad, A. Heydarinasab and M. Ardjmand, Adsorption of adenine on the surface of nickel-decorated graphene; A DFT study, *J. Alloys Compd.*, 2016, **686**, 662–668.
78 A. Shokuhi Rad, A. S. Alijantabar, N. Motaghedi, S. Maleki and M. Peyravi, Theoretical study of chemisorption of

cyanuric fluoride and S-triazine on the surface of Al-doped graphene, *Mol. Simul.*, 2016, **42**(18), 1519–1527.
79 A. S. Rad, Adsorption of mercaptopyridine on the surface of Al-and B-doped graphenes: Theoretical study, *J. Alloys Compd.*, 2016, **682**, 345–351.
80 M. Magdy, M. M. Aboelnga, A. Deyab, A. Semida, R. Rizk, N. Elseady, *et al.*, Experimental and theoretical investigations of divinylbenzene-based polymer as an efficient adsorbent for brilliant green dye removal, *RSC Adv.*, 2025, **15**(25), 19843–19858.
81 N. Samghouli, I. Bencheikh, K. Azoulay, S. Jansson and S. El Hajjaji, Mechanistic and reactional activation study of carbons destined for emerging pharmaceutical pollutant adsorption, *Environ. Monit. Assess.*, 2025, **197**(3), 259.
82 R. L. Tseng, Physical and chemical properties and adsorption type of activated carbon prepared from plum kernels by NaOH activation, *J. Hazard. Mater.*, 2007, **147**(3), 1020–1027.
83 D. Angin and S. Sarikulce, The effect of activation temperature on properties of activated carbon prepared from wine industry pressing waste, *Desalin. Water Treat.*, 2017, **73**, 373–379.
84 M. F. R. Pereira, S. F. Soares, J. J. M. Órfão and J. L. Figueiredo, Adsorption of dyes on activated carbons: influence of surface chemical groups, *Carbon N Y*, 2003, **41**(4), 811–821.
85 O. Pezoti, A. L. Cazetta, K. C. Bedin, L. S. Souza, A. C. Martins, T. L. Silva, *et al.*, NaOH-activated carbon of high surface area produced from guava seeds as a high-efficiency adsorbent for amoxicillin removal: Kinetic, isotherm and thermodynamic studies, *Chem. Eng. J.*, 2016, **288**, 778–788.
86 F. A. Ahangar, U. Rashid, J. Ahmad, T. Tsubota and A. Alsalme, Conversion of waste polyethylene terephthalate (Pet) polymer into activated carbon and its feasibility to produce green fuel, *Polymers*, 2021, **13**(22), 3952.
87 N. E. Williams, O. A. Oba and N. P. Aydinlik, Modification, production, and methods of KOH-activated carbon, *ChemBioEng Rev.*, 2022, **9**(2), 164–189.
88 M. N. Efimov, A. A. Vasilev, D. G. Muratov, A. I. Kostev, E. A. Kolesnikov, S. G. Kiseleva, *et al.*, Conversion of polyethylene terephthalate waste into high-yield porous carbon adsorbent *via* pyrolysis of dipotassium terephthalate, *Waste Manage.*, 2023, **162**, 113–122.
89 O. Alabi-Babalola, E. Aransiola, E. Asuquo, A. Garforth and C. D'Agostino, Production of Highly Efficient Activated Carbons for Wastewater Treatment from Post-Consumer PET Plastic Bottle Waste, *Chempluschem*, 2024, **89**(5), e202300484.
90 M. Efimov, A. Vasilev, D. Muratov, A. Panin, M. Malozovskaya and G. Karpacheva, Application of infrared pyrolysis and chemical post-activation in the conversion of polyethylene terephthalate waste into porous carbons for water purification, *Polymers*, 2024, **16**(7), 891.
91 F. T. Johra, J. W. Lee and W. G. Jung, Facile and safe graphene preparation on solution based platform, *J. Ind. Eng. Chem.*, 2014, **20**(5), 2883–2887.
92 N. A. El Essawy, S. M. Ali, H. A. Farag, A. H. Konsowa, M. Elnouby and H. A. Hamad, Green synthesis of graphene from recycled PET bottle wastes for use in the adsorption of dyes in aqueous solution, *Ecotoxicol. Environ. Saf.*, 2017, **145**, 57–68.
93 S. Sharma, G. Kalita, R. Hirano, S. M. Shinde, R. Papon, H. Ohtani, *et al.*, Synthesis of graphene crystals from solid waste plastic by chemical vapor deposition, *Carbon N Y*, 2014, **72**, 66–73.
94 A. Pavithra, R. A. Rakkesh, D. Durgalakshmi and S. Balakumar, Room temperature detection of hydrogen gas using graphene based conductometric gas sensor, *J. Nanosci. Nanotechnol.*, 2017, **17**(5), 3449–3453.
95 K. S. W. Sing and R. T. Williams, Empirical procedures for the analysis of physisorption isotherms, *Adsorpt. Sci. Technol.*, 2005, **23**(10), 839–853.
96 J. Rouquerol, D. Avnir, C. W. Fairbridge, D. H. Everett, J. M. Haynes, N. Pernicone, *et al.*, Recommendations for the characterization of porous solids (Technical Report), *Pure Appl. Chem.*, 1994, **66**(8), 1739–1758.
97 A. Thakur and H. Kaur, Response surface optimization of Rhodamine B dye removal using paper industry waste as adsorbent, *Int. J. Ind. Chem.*, 2017, **8**(2), 175–186.
98 M. T. Uddin, M. A. Rahman, M. Rukanuzzaman and M. A. Islam, A potential low cost adsorbent for the removal of cationic dyes from aqueous solutions, *Appl. Water Sci.*, 2017, **7**(6), 2831–2842.
99 I. A. W. Tan, A. La Ahmad and B. H. Hameed, Adsorption of basic dye on high-surface-area activated carbon prepared from coconut husk: Equilibrium, kinetic and thermodynamic studies, *J. Hazard. Mater.*, 2008, **154**(1–3), 337–346.
100 B. Wang, W. Zhang, Y. Fu, Y. Wang and S. Hao, Case report: Ioversol induced Kounis syndrome and cardiogenic shock, *Heliyon*, 2023, **9**(4), e14742.
101 J. Galán, A. Rodríguez, J. M. Gómez, S. J. Allen and G. M. Walker, Reactive dye adsorption onto a novel mesoporous carbon, *Chem. Eng. J.*, 2013, **219**, 62–68.
102 T. M. Budnyak, M. Błachnio, A. Slabon, A. Jaworski, V. A. Tertykh, A. Deryło-Marczewska, *et al.*, Chitosan deposited onto fumed silica surface as sustainable hybrid biosorbent for acid orange 8 dye capture: Effect of temperature in adsorption equilibrium and kinetics, *J. Phys. Chem. C*, 2020, **124**(28), 15312–15323.
103 Y. A. Aggour, E. R. Kenawy, M. Magdy and E. Elbayoumy, Multifunctional copolymers for brilliant green dye removal: adsorption kinetics, isotherm and process optimization, *Environ. Sci.:Adv.*, 2025, **4**(5), 787–808.
104 K. S. Baidya and U. Kumar, Adsorption of brilliant green dye from aqueous solution onto chemically modified areca nut husk, *S. Afr. J. Chem. Eng.*, 2021, **35**, 33–43.
105 A. Soltani, M. Faramarzi and S. A. Mousavi Parsa, A review on adsorbent parameters for removal of dye products from

industrial wastewater, *Water Qual. Res. J.*, 2021, **56**(4), 181–193.

106 M. Magdy, M. M. Aboelnga, A. Deyab, A. Semida, R. Rizk, N. Elseady, *et al.*, Experimental and theoretical investigations of divinylbenzene-based polymer as an efficient adsorbent for brilliant green dye removal, *RSC Adv.*, 2025, **15**(25), 19843–19858.

107 S. Sadeghy, S. M. Pormazar, M. T. Ghaneian, M. H. Ehrampoush and A. Dalvand, Modeling and optimization of direct dyes removal from aqueous solutions using activated carbon produced from sesame shell waste, *Sci. Rep.*, 2024, **14**(1), 24867.

108 A. Bonilla-Petriciolet, D. I. Mendoza-Castillo and H. E. Reynel-Ávila. *Adsorption Processes for Water Treatment and Purification*, Springer, Vol. 256, 2017.

109 N. A. Rahman, M. Ajiza, D. A. Anggorowati, F. E. K. Rastini and L. Mustiadi, Clove leaf distillation using briquette fuel with starch and molasses as a binder, *Mater. Today: Proc.*, 2022, **63**, S293–S296.

110 N. Ayawei, A. N. Ebelegi and D. Wankasi, Modelling and interpretation of adsorption isotherms, *J Chem*, 2017, **2017**(1), 3039817.

111 V. O. Shikuku and T. Mishra, Adsorption isotherm modeling for methylene blue removal onto magnetic kaolinite clay: a comparison of two-parameter isotherms, *Appl. Water Sci.*, 2021, **11**(6), 103.

112 H. Swenson and N. P. Stadie, Langmuir's theory of adsorption: A centennial review, *Langmuir*, 2019, **35**(16), 5409–5426.

113 U. A. Edet and A. O. Ifelebuegu, Kinetics, isotherms, and thermodynamic modeling of the adsorption of phosphates from model wastewater using recycled brick waste, *Processes*, 2020, **8**, 665.

114 M. Saxena, N. Sharma and R. Saxena, Highly efficient and rapid removal of a toxic dye: adsorption kinetics, isotherm, and mechanism studies on functionalized multiwalled carbon nanotubes, *Surf. Interfaces*, 2020, **21**, 100639.

115 N. E. Richey, C. De Paula and S. F. Bent, Understanding chemical and physical mechanisms in atomic layer deposition, *J. Chem. Phys.*, 2020, **152**(4), 1–17.

116 N. M. Aljamali, R. Khdur and I. O. Alfatlawi, Physical and chemical adsorption and its applications, *Int. j. Thermodyn. Chem. Kinet.*, 2021, **7**(2), 1–8.

117 K. L. Yu, X. J. Lee, H. C. Ong, W. H. Chen, J. S. Chang, C. S. Lin, *et al.*, Adsorptive removal of cationic methylene blue and anionic Congo red dyes using wet-torrefied microalgal biochar: Equilibrium, kinetic and mechanism modeling, *Environ. Pollut.*, 2021, **272**, 115986.

118 E. D. Revellame, D. L. Fortela, W. Sharp, R. Hernandez and M. E. Zappi, Adsorption kinetic modeling using pseudo-first order and pseudo-second order rate laws: A review, *Clean Eng Technol.*, 2020, **1**, 100032.

119 M. G. El-Desouky, A. A. Alayyafi, G. A. A. M. Al-Hazmi and A. A. El-Bindary, Effect of metal organic framework alginate aerogel composite sponge on adsorption of tartrazine from aqueous solutions: adsorption models, thermodynamics and optimization *via* Box-Behnken design, *J. Mol. Liq.*, 2024, **399**, 124392.

120 S. P. Sun and A. T. Lemley, p-Nitrophenol degradation by a heterogeneous Fenton-like reaction on nano-magnetite: Process optimization, kinetics, and degradation pathways, *J Mol Catal A Chem*, 2011, **349**(1), 71–79.

121 D. Azzouni, F. Baragh, A. M. Mahmoud, M. M. Alanazi, Z. Rais and M. Taleb, Optimization of methylene blue removal from aqueous solutions using activated carbon derived from coffee ground pyrolysis: A response surface methodology (RSM) approach for natural and cost-effective adsorption, *J. Saudi Chem. Soc.*, 2023, **27**(5), 101695.

122 S. M. Beyan, S. V. Prabhu, T. T. Sissay and A. A. Getahun, Sugarcane bagasse based activated carbon preparation and its adsorption efficacy on removal of BOD and COD from textile effluents: RSM based modeling, optimization and kinetic aspects, *Bioresour. Technol. Rep.*, 2021, **14**, 100664.

123 J. Yu, L. Bai, Z. Feng, L. Chen, S. Xu and Y. Wang, Waste treats waste: Facile fabrication of porous adsorbents from recycled PET and sodium alginate for efficient dye removal, *Chemosphere*, 2024, **355**, 141738.

124 B. Abbou, I. Lebkiri, H. Ouaddari, A. El Amri, F. E. Achibat, L. Kadiri, *et al.*, Improved removal of methyl orange dye by adsorption using modified clay: combined experimental study using surface response methodology, *Inorg. Chem. Commun.*, 2023, **155**, 111127.

125 M. A. Ahmad and R. Alrozi, Optimization of preparation conditions for mangosteen peel-based activated carbons for the removal of Remazol Brilliant Blue R using response surface methodology, *Chem. Eng. J.*, 2010, **165**(3), 883–890.

126 I. A. W. Tan, A. La Ahmad and B. H. Hameed, Adsorption of basic dye on high-surface-area activated carbon prepared from coconut husk: Equilibrium, kinetic and thermodynamic studies, *J. Hazard. Mater.*, 2008, **154**(1–3), 337–346.

127 P. Samiyammal, A. Kokila, L. A. Pragasan, R. Rajagopal, R. Sathya, S. Ragupathy, *et al.*, Adsorption of brilliant green dye onto activated carbon prepared from cashew nut shell by KOH activation: Studies on equilibrium isotherm, *Environ. Res.*, 2022, **212**, 113497.

128 O. Aladeokin and A. Fletcher, A novel activated carbon material from peanut shells for the removal of methyl orange and methylene blue dyes from wastewater: Kinetics, isotherms and mechanism, *Adsorpt. Sci. Technol.*, 2024, **42**, 02636174241256843.

129 M. K. Gupta, P. K. Tandon, N. Shukla, H. Singh and S. Srivastava, Efficient removal of methyl orange and rhodamine-B dyes with low cost banana peel activated carbon, *Asian J. Chem.*, 2020, **32**(5), 1121–1127.